LINKAGE BETWEEN LOWER PENNSYLVANIAN SANDSTONE DIAGENESIS AND CARBON SEQUESTRATION RESERVOIR QUALITY IN RUSSELL COUNTY, VIRGINIA

Joyce E. Carbaugh

Thesis submitted to the Faculty of

Virginia Polytechnic Institute and State University

in partial fulfillment of the requirements for the degree of

MASTER OF SCIENCE

in

GEOSCIENCES

Kenneth A. Eriksson, Chair

J. Fred Read

Michal Kowalewski

July 26, 2011

Blacksburg, Virginia

Keywords: petrography, diagenesis, Lower Pennsylvanian, carbon sequestration, reservoir quality

LINKAGE BETWEEN LOWER PENNSYLVANIAN SANDSTONE DIAGENESIS AND CARBON SEQUESTRATION RESERVOIR QUALITY IN RUSSELL COUNTY, VIRGINIA

Joyce E. Carbaugh

ABSTRACT

An enhanced coal-bed methane facility in Russell County, Virginia is targeting lower Pennsylvanian coals for CO_2 storage, but the shallow sandstone units intercalated with the coals may also prove to be potential CO_2 reservoirs, since the injection apparatus is already in place. Using samples from a continuous core in southwestern Virginia, this detailed review of the petrography and local volume of the Breathitt Formation sandstone units examines their diagenetic alterations in order to assess the units' reservoir quality.

The high-frequency sequences of immature sandstones, heterolithics, shales and coals in Russell County represent deposits from the transverse fluvial facies association of a broad braided-fluvial drainage system in the central Appalachian Basin. The sandstone units within these sequences are laterally extensive, maintaining similar thickness and gamma ray signature across the study area.

Lower Pennsylvanian sandstone units are consistently sublitharenite with a diagenetic mineral assemblage including siderite, chlorite, kaolinite, albite, illite, silica and calcite. Primary porosity is not preserved, but secondary porosity (5 ± 3.1 %) has developed at the expense of feldspars and unstable lithic fragments. Permeability assessments collected in Grimm (**2010**) measured impervious values (0.005-0.008mD) for the medium-coarse grained sublitharenites.

At the temperatures and pressures present within these units, CO_2 is unlikely to react with either the primary or diagenetic mineralogy in a way that negatively impacts continued injection on human time scales. Low pore volume and permeability due to the timing of certain authigenic mineral emplacement are the main hindrance to reservoir quality. Lower Pennsylvanian sandstones are not viable potential reservoirs for carbon sequestration.

ACKNOWLEDGEMENTS

Firstly, I would like to thank my advisor Ken Eriksson for his guidance through my graduate career, and thoughtful editing and much needed critical review on this thesis. Additionally, my committee members, Fred Read and Michal Kowalewski, had keen insights to improve this project and scheduling flexibility for which I am very grateful.

I would like to recognize the organizations that supported this project by the donations of data:

Virginia Center for Coal & Energy Research (VCCER)
Equitable Resources (EQR)

as well as those organizations that provided funding:

ConocoPhillips
AAPG Grants-In-Aid Program
Virginia Tech Department of Geosciences

The faculty, staff, and students of the Virginia Tech Department of Geosciences have time and time again impressed me with their academic prowess and cheerful camaraderie. I am grateful for the many friends I have made here, but particularly my office colleagues in the Centre for Sedimentology & Stratigraphic Excellence. I thank Ryan Grimm, Tina Blue, Bill Rouse and Adeola Oyewumi for their remarkable openness to impromptu technical discussions, willingness to field questions, and generosity with much needed support and friendship. Of course, I would like to extend many, many thanks to the fairy godmothers of the Administrative Staff who make the magic happen every day.

Much credit for the completion of this thesis is due to the listening ears of my loving family and my long-suffering fiancé. Their steadfast support has been the foundation for all of my academic endeavors, and without their encouragement this achievement could not have been reached. This thesis is dedicated to them.

Partial funding for this project provided by the 2009-2010 ConocoPhillips Graduate Student Fellowship

All photographs taken by author unless otherwise noted.

Table of Contents

LIST OF FIGURES

LIST OF TABLES

INTRODUCTION

The current geographic and stratigraphic locations of Lower Pennsylvanian sandstones make them candidates for carbon sequestration reservoirs. An enhanced coal-bed methane facility targeting lower Pennsylvanian coals for hydrocarbon extraction and CO_2 storage has recently begun testing and operations in Russell County, Virginia. A series of successful CO_2 injections into the coals has taken place over the last four years, and has been carefully assessed at several on-site monitoring wells (**Kaszuba et al., 2005; Ripepi, 2009**). Eighteen-hundred feet of continuous core from a monitoring well within the injection facility contains samples of coarse sandstone units intercalated with the targeted coals. With the upfront costs typically required to access these sandstones largely completed, these sandstones' potential porosity and proximity to the coals highlight them as prospective CO_2 reservoirs.

The purpose of this study is to evaluate factors that have influenced diagenesis and their effects on reservoir quality in the lower Pennsylvanian sandstones in the central Appalachian basin around Russell County, Virginia (**Fig. 1**) using petrography within the subsurface stratigraphic framework. The discipline of sandstone diagenesis is strongly tied to studies involving reservoir property evaluation and quality prediction, thus reservoir quality assessment can benefit from a detailed understanding of the controls on diagenesis (**e.g. Wilson, 1994; Primmer et al., 1997; Jeans, 2000**). Integrating data from various scales is a valuable asset to develop a comprehensive understanding of the diagenetic histories of sedimentary basins. To accomplish this, this study (1) undertakes subsurface mapping to construct a framework for sandstone bodies and associated mudstones and coals; and (2) contrasts their primary and diagenetic mineralogy to assess available porosity of sandstone bodies by using samples from a

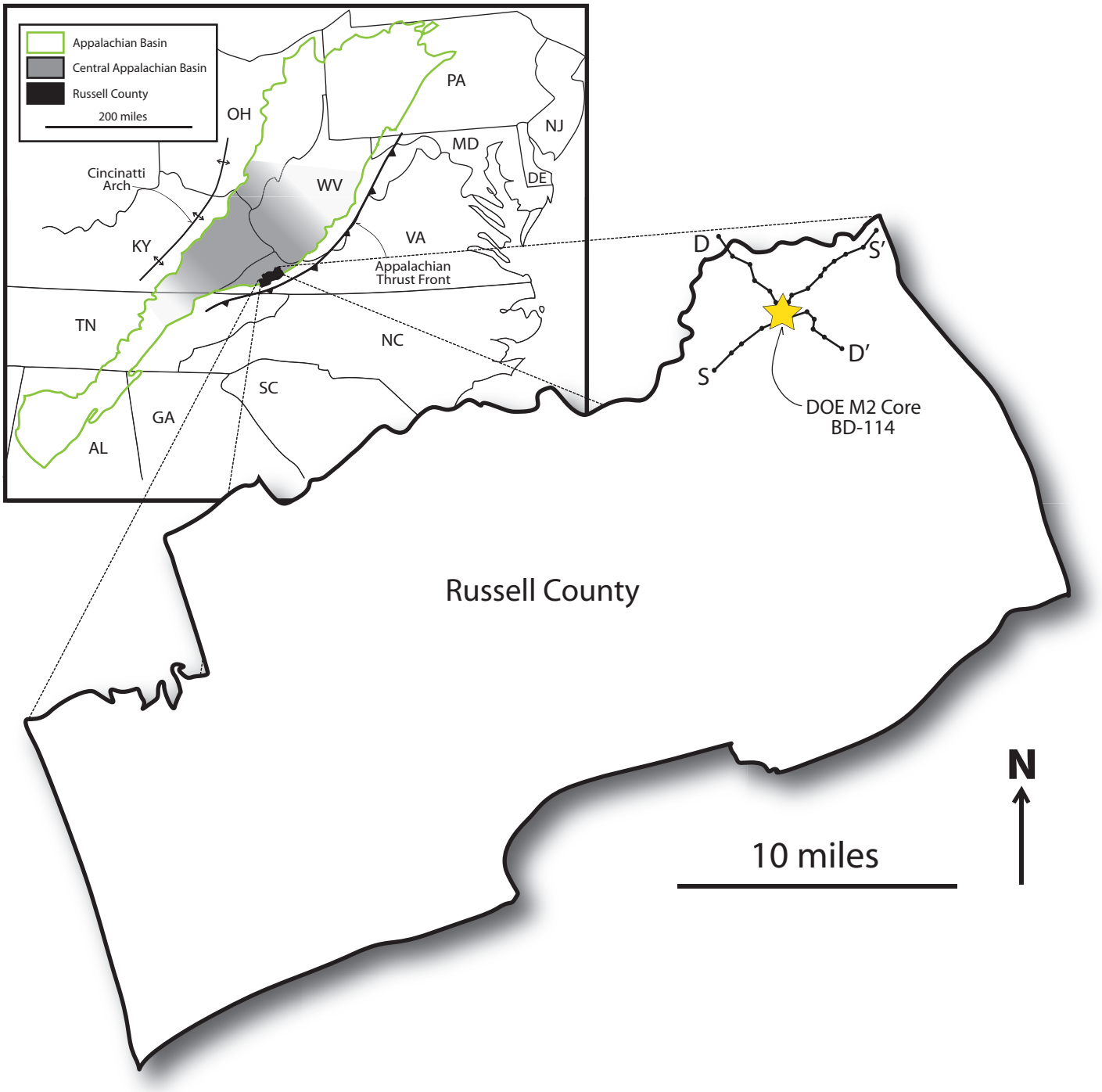

Figure 1: Regional Map of Study Area. Inset map showing location of central Appalachian basin, bounding structures, and Russell County, Virginia. Enlarged map of Russell County shows the location of DOE M2 well and strike- and dip-parallel cross-sections S-S' and D-D'. (Adapted from Quinlan and Beaumont, 1984; Chesnut, 1994; Korus, 2002; Bodek, 2006)

continuous core. A literature review complements the above analyses, focusing on the dominant modes and challenges of geological carbon sequestration of carbon dioxide.

The strata beneath southwestern Virginia were deposited in a hinterland-thickening wedge of fluvial and alluvial environments as the active Appalachian Thrust Front shed a pulsing flux of weathered detritus into the foreland basin (**Ferm, 1974; Donaldson, 1985; Englund and Thomas, 1990; Allen, 1993; Greb and Chesnut, 1996; Grimm, 2010**). The preserved basin-fill consists of a heterogeneous suite of siliciclastic strata and coal beds intercalated with broad quartz arenite belts (**Chesnut, 1996; Greb et al., 2008**). The laterally-extensive sandstone bodies which are the focus of this study vary in framework composition from quartz arenite to lithic, with a varied suite of secondary alterations (**Reed et al., 2005a; Grimm, 2010**).

Subsurface stratigraphy in this project focuses on a six-kilometer radius around the well site, utilizing the abundance of gamma ray logs drilled in this region for coal exploration. Focused interpretations on the local lithologies are made by correlating these data in two cross-sections, aligned to the structural strike and dip of the basin. On the largest scale, subsurface stratigraphy data connects this work with other regionally-based studies (**Arkle, 1974; Reed et al., 2005a,b; Grimm, 2010**), and forms the context for finer scale investigation. For reservoir quality, the continuity and bulk volume of the sandstone bodies were determined from gamma ray logs (**Bodek, 2006; Denning, 2008; Rouse, 2009**).

In a succession as heterolithic as the lower Pennsylvanian of the central Appalachian Basin, constraining the sandstone composition refines diagenetic history evaluations. Multistage burial and diagenetic histories of these units have produced considerable amounts of altered secondary minerals and porosity (**Houseknecht, 1980; Reed et al., 2005a**). Petrographic examination at the millimeter and micrometer scale allows a documentation of framework

mineralogy (**De Ros et al., 1994; von Eynatten, et al., 2003**). It yields an evaluation of secondary minerals, which reveals the burial and diagenetic histories (**de Souza et al., 1995; Hiatt and Kyser, 2000; Milliken, 2003; Reed et al., 2005b**). Petrography allows for an analysis of clay mineral formation and fluid flow history, and a quantitative assessment of the porosity of the units (**Houseknecht, 1978**).

GEOLOGIC BACKGROUND

Appalachian Basin strata trend northeast-southwest along eastern North America from New York to Alabama, separated into subbasins based on structures and varying composition (**Donaldson et al., 1985**). The central region of the Appalachian basin in Virginia, West Virginia, Kentucky and Tennessee, is bound to the east by the Appalachian Valley and Ridge Province and to the west by the Cincinnati Arch (**Fig. 1**). In the southeast, the late Mississippian Bluestone Formation is unconformably overlain by early Pennsylvanian sedimentary rocks of the Breathitt Group, a clastic wedge up to 900 meters thick (**Fig. 2**) (**Englund et al., 1979; Englund and Thomas, 1990; Korus, 2002; Blake and Beuthin, 2008**). The Lower Pennsylvanian suite in the central Appalachian Basin includes heterolithic and coal-bearing units, which have been widely studied both in outcrop and the subsurface (**Chesnut, 1996; Korus, 2002; Bodek, 2006; Denning, 2008; Ripepi, 2009; Rouse, 2009; Grimm, 2010**).

Structural History

Convergent tectonic episodes in the Paleozoic Taconic, Acadian, and Alleghanian orogenies produced the Appalachian foreland basin structures and strata. The Alleghanian orogeny (late Mississippian to Permian), during the collision of Africa and eastern North America during the assembly of Pangaea in the Carboniferous-Permian, had the greatest influence on late Paleozoic Appalachian basin formation (**Hatcher, 2002; Blakey, 2008**). Plate reconstructions suggest that the Appalachian Basin was situated in sub-equatorial latitudes during the Pennsylvanian and trended east-west with the Alleghanian highlands along the southern margin (**Van der Voo, 1983; Quinlan and Beaumont, 1984; Scotese, 2004; Blakey, 2008**).

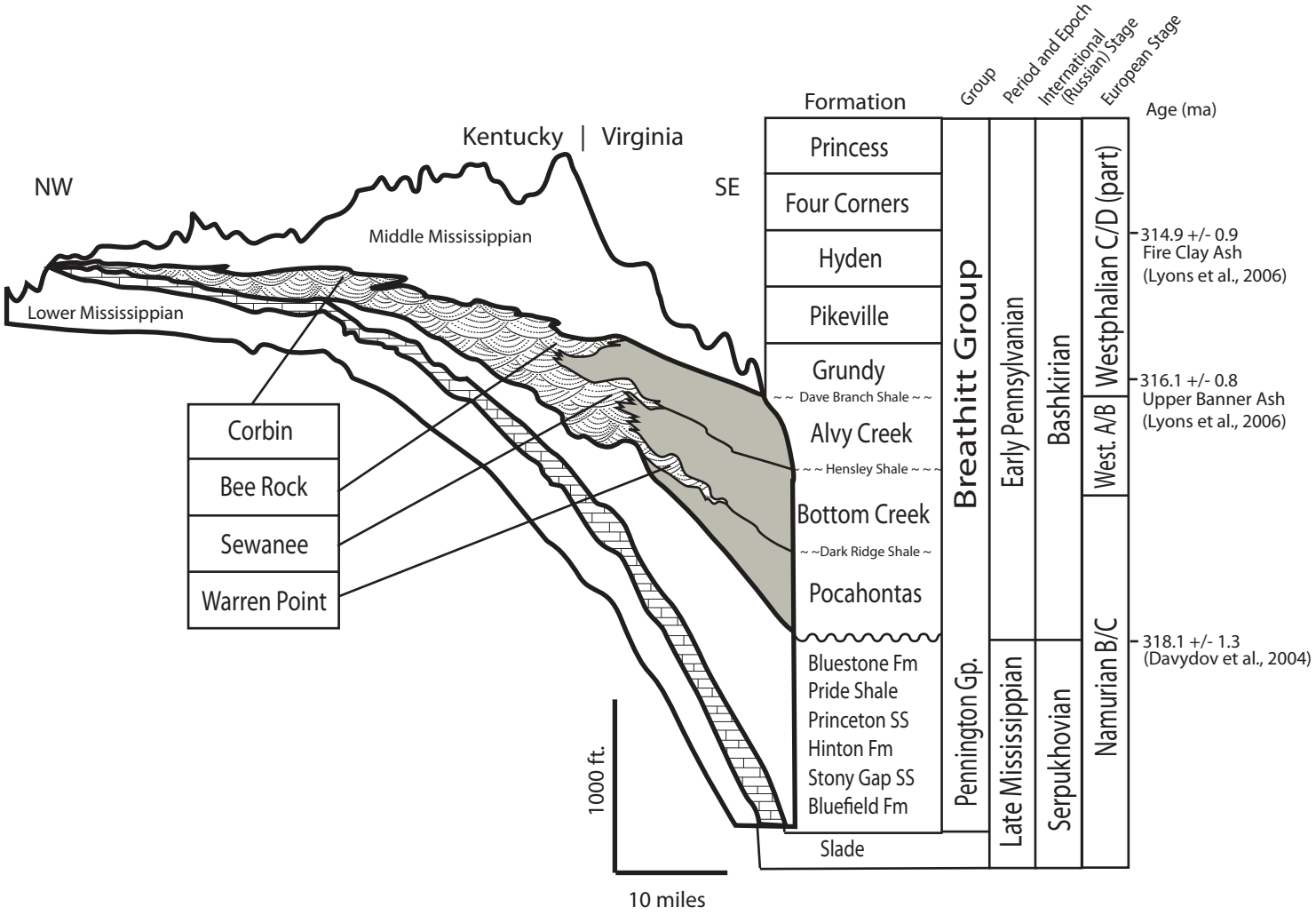

Figure 2: Schematic Cross-section and Correlation Chart. Schematic cross-section showing the vertical succession, generalized geometry and distribution of Upper Mississippian shales and the Lower-Mid Pennsylvanian Breathitt Group. Correlative period and global stage boundaries are listed alongside the schematic diagram for further explanation. (Adapted from Englund and Thomas, 1990; Chesnut, 1994; Davydov et al., 2004; Greb and Martino, 2005; Bodek, 2006)

Lithospheric flexure in response to successive thrust-loading events controlled the basin geometry on both short and long time scales. Long-term downwarping of the crust resulted in a wedge of sedimentary rocks thickening toward the thrust front (**Fig. 2**), typical of foreland basins (**Dickinson and Suczek, 1979; Castle, 2001**). Short-term flexure shaped patterns in the stratigraphic architecture of orogen- and craton-derived sedimentation, as subsidence related to individual tectonic events ensued (**Tankard, 1986; Grimm, 2010).** The overall flexural rigidity of the crust during the Alleghanian orogeny resulted in a relatively broad, shallow basin which filled with cycles of heterogeneous siliciclastic detritus (**Tankard, 1986**, **Klein and Willard, 1989**).

Stratigraphic Framework

Interfingering facies belts in Lower Pennsylvanian strata include a heterolithic coal-bearing facies belt to the southeast, which passes into a quartz arenite facies belt to the northwest (**Fig. 2**). The transition between these units varies from an abrupt to a gentle gradation pattern (**Englund, 1974**). Toward the southeast, the thickest units of the Lower Pennsylvanian clastic wedge are the Pocahontas, Bottom Creek, Alvy Creek and Grundy Formations of the Breathitt Group. These lithostratigraphic units are oriented parallel to basin structural dip, and are characterized by lithic-rich sandstone, siltstone, shale, clay and coal, with Alleghanian highland provenance (**Englund et al., 1986; Rice, 1985; Rice and Schwietering, 1988**). Toward the northwest, the Breathitt Group strata are intercalated with the Warren Point, Sewanee, and Bee Rock sandstone members of the Lee Formation (**Rice and Schwietering, 1988; Chesnut, 1994**). The Lee Formation is a quartz arenite that trends parallel to the basin axis and contains sediment sourced from recycled older Paleozoic strata and the much older North American craton (**Houseknecht, 1980; Reed et al., 2005a**).

Eight third-order sequences in the Breathitt Group are characterized by extensive marine shale horizons grading up to coarser, heterolithic strata. The study interval contains at least four of these sequences, subdivided by the Dark Ridge, Hensley and Dave Branch shales (**Chesnut, 1994**). Timing of deposition is constrained by tonsteins in the Fire Clay and Upper Banner coals (**Fig. 2**). Volcanic-sourced zircons have been dated at 314.6 ± 0.9 Ma using U-Pb techniques in the Fire Clay coal (**Lyons et al., 2006**), and sanidines containing $^{40}Ar/^{39}Ar$ have dated the Upper Banner coal 316.1 ± 0.8 Ma (**Lyons et al., 1997**). Davydov et al. (**2004**) set the Serpukhovian-Bashkirian boundary in the Pennsylvanian at 318.1 ± 1.3 Ma, an age that has been associated with the unconformity at the base of the Pennsylvanian in the central Appalachian Basin.

The mature sandstone units of the Lee Formation are interpreted as long-lasting braided river deposits, from a cratonic watershed (**Houseknecht, 1980; Rice, 1985; Rice and Schwietering, 1988; Archer and Greb, 1995; Greb and Chesnut, 1996; Eriksson et al., 2004**). As the axial trunk stream carried mature sediment southwest, it converged with transverse tributaries carrying immature sediments of the Breathitt Group directly from the metamorphic terranes of the thrust front to the southeast (**Fig. 3**) (**Davis and Ehrlich, 1974, Houseknecht, 1980; Korus, 2002; Reed et al., 2005a**). The resulting stratigraphic architecture is a result of both tectonic and eustatic influences on accommodation. Tectonic pulses increased sediment supply and induced subsidence-derived accommodation space (**Tankard, 1986; Grimm, 2010**). During eustatic sea level rise, the transgressed fluvial systems developed into broad estuaries, which prograded into small, fluvial-dominated deltas during subsequent regression and accommodation increase (**Greb and Chesnut, 1996; Bodek, 2006; Korus et al., 2008**). Located in a sub-equatorial region, the climate during deposition was quite warm, fostering the

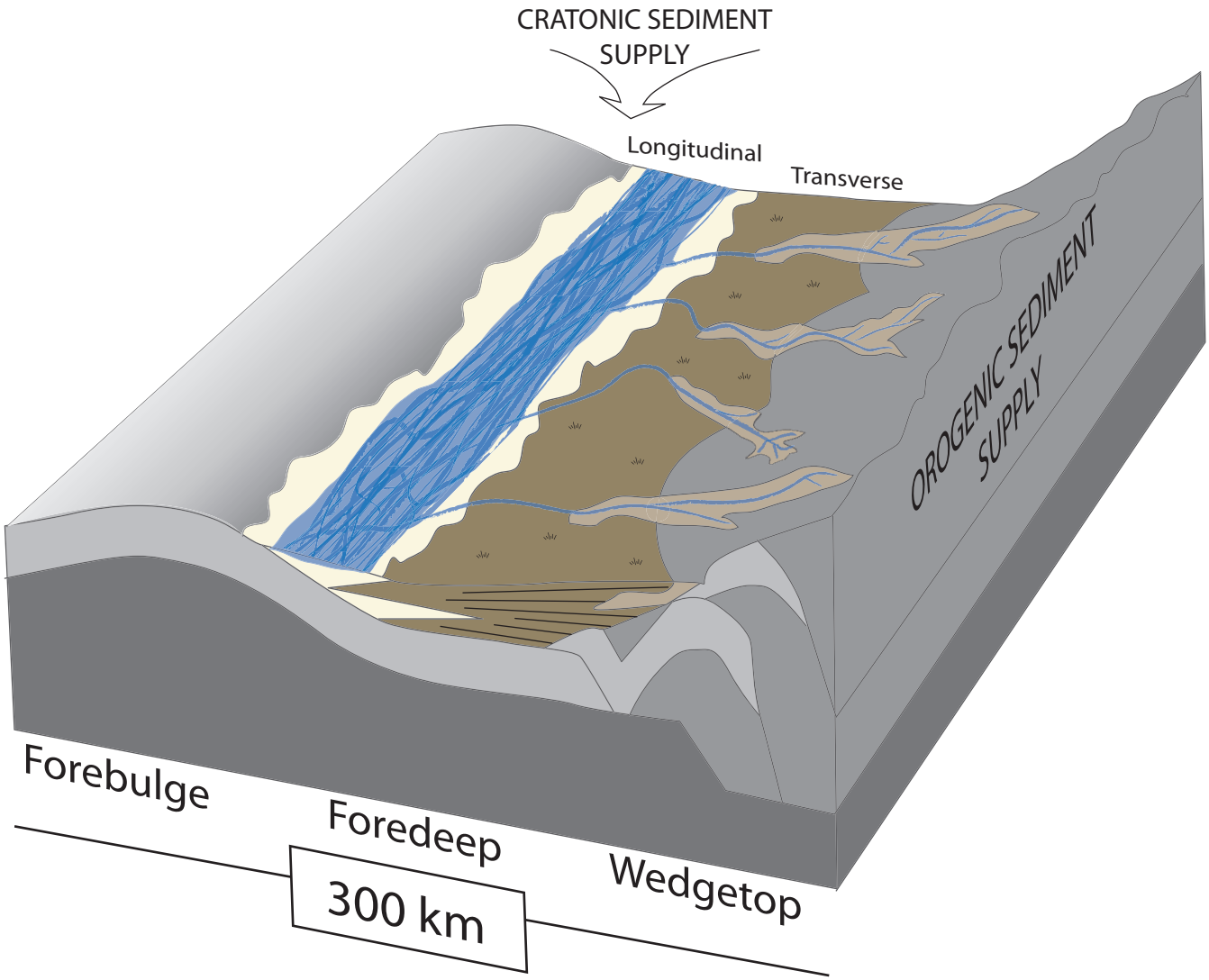

Figure 3: Depositional Environment Block Diagram. Generalized depositional model for lower Pennsylvanian strata in the study area illustrating coexisting longitudinal and transverse fluvial depositional systems. (Adapted from Bodek, 2006; Grimm, 2010)

development of swampy, organic-rich environments, preserved as abundant coal beds and black shales in the Bottom Creek, Alvy Creek and Pocahontas formations.

The abundant coal beds in the Breathitt Group are currently targeted for enhanced hydrocarbon extraction. The associated immature sandstone bodies are the focus of this study because the core, located close to the southeastern basin margin, only samples Breathitt Group formations. These units are more varied than the quartzarenite Lee Formation sandstones, but the heterogeneity is potentially more advantageous: more varied diagenetic histories in the sandstones, and repetitive shales as potential confining units for seal evaluation and enhanced coalbed methane extraction (**Grimm, 2010**).

Previous Work on Petrography

There is a high degree of lateral variation in the ratios of quartz, feldspars and lithic fragments due to the fluvial deposition of the sandstones within the central Appalachian basin (**Davis and Ehrlich, 1974**). The most quartz-rich facies are located along strike, farthest from the Appalachian Thrust Front, associated with the trunk-stream deposits of the Lee Formation and the Pottsville Group (**Siever, 1957; Chen and Goodell, 1964; Houseknecht, 1980; Wizevich, 1991; Grimm, 2010**). Feldspar concentrations in the sandstones are consistently low, but increase along strike toward southern West Virginia, southwest Virginia and eastern Kentucky, especially with respect to perthitic textures (**Davis and Ehrlich, 1974; Milliken, 2001; Reed et al., 2005a**). This distribution has been attributed to the dissection of the cratonic source down to its plutonic root (**Davis and Ehrlich, 1974**). The lithic components of these sandstones are largely metamorphic rock fragments recycled from the rising Alleghanian orogen, and are in peak abundance along the southeastern part of the basin (**Houseknecht, 1980; Dickinson et al., 1983; Donaldson et al., 1985; McDowell, 1986**).

Secondary mineral abundances also display significant variability in this region, and requiring a substantial sample set to ground an interpretation (**Milliken, 2001**). Reed and others (**2005a**) conducted an intensive petrographic analysis of 186 Pennsylvanian samples largely from West Virginia, and interpreted the presence and absence of secondary minerals and cements into the following paragenesis, starting with earliest emplacement during burial: siderite, ferric oxyhydroxide, chlorite, kaolinite, calcite, albite, illite, quartz, porosity development, and dolomite. They found that secondary alteration and porosity mainly occurred at the expense of feldspars and ductile rock fragments, which formed extensive pseudomatrix in the lithic arenite samples. The authors concluded that framework grain composition was the most significant control on diagenesis in these strata, rather than pore fluid origin.

Burial History

Sediments deposited in foreland basins are buried quickly due to rapid subsidence. The lower Pennsylvanian Breathitt Group reached its maximum burial depth of 4.5 km with a geothermal gradient of 30 ^{o}C/km at 274 ± 4 Ma, which is about 44 m.y. after deposition (**Miller and Kent, 1988; Levine and Davis, 1989; Blackmer, 1994; Reed et al., 2005b**). Upper Pennsylvanian sandstones experienced advective flow of warm, silica-rich fluids at 70 km from the thrust front, recorded by a disparity between 70 ^{o}C difference between vitrinite reflectance and fluid inclusion microthermometry results. Lower Pennsylvanian sandstones record no injection of warm fluids in the vitrinite or fluid inclusions, but the presence of silica-enriched fluid may be the source for the minor amounts of silica cement in the Breathitt Group (**Reed, 2003; Ruppert et al., 2010**).

Three stages of exhumation were derived from Apatite Fission Track and (U-Th)/He ages (**Reed et al., 2005b**). AFT data support the first phase of exhumation, from maximum burial to

~3.1 km depth, at a rate of ~10 m/m.y. by the early Cretaceous. The second phase, constrained by (U-Th)/He ages, the basin was exhumed to a depth of ~1.7 km at a rate of ~30 m/m.y (**Boettcher and Milliken, 1994**). The third phase is also constrained by (U-Th)/He ages, and exhumed these strata to 0.4 km above sea level, at the same rate as the second phase (**Reed et al., 2005b**).

METHODOLOGY

Core data is avoids the damaging effects of surface weathering, keeping the character of the rock at depth. The focal point of this study, DOE M2 core, is associated with injection well BD-114 in Russell County, Virginia. The Department of Energy commissioned this core to a depth of 2200 ft, which was later donated to Virginia Tech, minus the coal intervals. The sampled array intersects all major lithologies of the Breathitt Group. Using samples selected exclusively from this core, data was collected at three scales, each at least one order of magnitude removed from the next.

Well-log attributes and cross-section construction

The stratigraphic framework was constructed using 23 gamma ray wireline logs, compiled from digitally accessible natural gas development wells. Both SW-NE strike-oriented and SE-NW dip-oriented cross-sections were constructed, intersecting at the core site. The DOE M2 core was logged, and its gamma ray and bulk density logs were used to apply lithologic interpretations of other wireline logs without core data. Distinctive gamma ray and bulk density responses and patterns for lower Pennsylvanian units were recognized based on core-to-log observations and Grimm (**2010**). Coals were used for regional correlations using their low density relative to siliciclastic lithologies. The Hensley Shale was used as the regional datum to hang all the logs. Cross-sections were constructed using Halliburton's GeoGraphix software package and were further enhanced by Adobe Illustrator, commercial image editing software.

Petrographic Data Collection and Cathodoluminescence Analysis

Samples for analysis were selected from the top, middle and base of each large, continuous sandstone bodies, in order to counteract the effects of differential diagenesis near

shale contacts (**Galloway, 1974; McBride, 1989**). Thin-section billets were processed by Spectrum Petrographics, where they were stained with stain Kferricyanide for potassium feldspar, Alzarin-red for calcite, and impregnated with blue epoxy. Samples were examined under a Nikon polarizing microscope equipped with a Leitz mechanical stage. Framework and secondary mineralogies were identified at a 200-count density on 52 slides. Point-count procedures used were according to Glagolev-Chayes method (**Galehouse, 1971**). Translation interval remained constant at 2mm throughout to accommodate the largest mean grain sizes. Framework grain, authigenic mineral, and cement composition as well as pore space from each of the slides was tabulated onto a data sheet (**Appendix A**). Qualitative analysis was necessary to analyze the textural relationships between cements, framework grains and pseudomatrix in combination with more quantitative methods.

Cathodoluminescent images of the carbonate cements and feldspar grains were obtained using a Citl CCL 8200 Mk4 analyzer. Beam conditions were set at a 600 μA beam current and 10.0 kV acceleration potential at an average working distance of 22 mm. Digital panchromatic images were taken over scan times of 1 to 5 minutes.

Scanning Electron Microprobe Data Collection

Selected carbonate cements and feldspar grains were examined for mineral chemistry to pinpoint mineralogy and formation conditions using the CAMECA SX-50/SUN 3/160 electron probe microanalyzer at Virginia Tech. Carbonate cements were evaluated to identify their heavier components, using hematite (Fe), pyrolusite (Mn), wollastonite (Ca) and olivine (Mg; Marjalahti) standards. Feldspar was analyzed to constrain the abundance of albite, using Na feldspar (Na; Amelia), wollastonite (Si, Ca), kyanite (Al), orthoclase (K; Benson), hematite(Fe) standards. Acceleration potential and sample current were set at 15.0 kV and 20.0 nA

respectively. Chemical spot analyses using EDS analysis system on the SEM yielded elemental ratios which helped confirm mineral identifications for carbonates and feldspars.

RESULTS – REGIONAL LITHOLOGY

Lithologic Summary

All logged lithologies from the DOE M2 core were grouped into four facies categories: Sandstone, heterolithic, mudstone, and coal. Descriptions follow for each category.

Sandstone bodies: In the M2 core (**Fig. 4**), these are medium gray, and are comprised of fine-to-coarse, subangular to subrounded and moderately sorted grains. The sandstones are classified as sublitharenites due to the presence of metamorphic schistose fragments, polycrystalline quartz, biotite, micas, and feldspars (see next chapter for more detail). Sedimentary structures are limited in the sampled sandstones. Most sandstone units are massive in texture, but some thinner units exhibit obvious planar bedding. No cross-bedding is observed in the core-sampled sandstones, but such structures are difficult to identify on core-sample scale. Major sandstone units vary in thickness from 2 - 10 m over the depth intersected by the core. There is a generalized trend of decreasing sandstone thickness with depth. The shallower units tend to be thicker and more uniform than the deeper sandstone units. Deeper sandstone units are thinner and more frequently separated by finer-grained units and coals. Basal siderite and shale fragments are common in sandstone units bounded by finer-grained siliciclastic material. The shale fragments are commonly elongate in shape and similar in composition to underlying finer grained lithologies. Carbonized plant debris is common, but no body fossils are found in any of these samples. However, the coarse-grained nature of the sample set does not preferentially preserve fossils.

Heterolithic units: These are comprised of thinly intercalated beds of mudstone, siltstone, and sandstone. Muddy heterolithic units intercalated with the sandstone units show perturbed bedding such as burrows and root casts, but this is not present in the coarser grained sandstones.

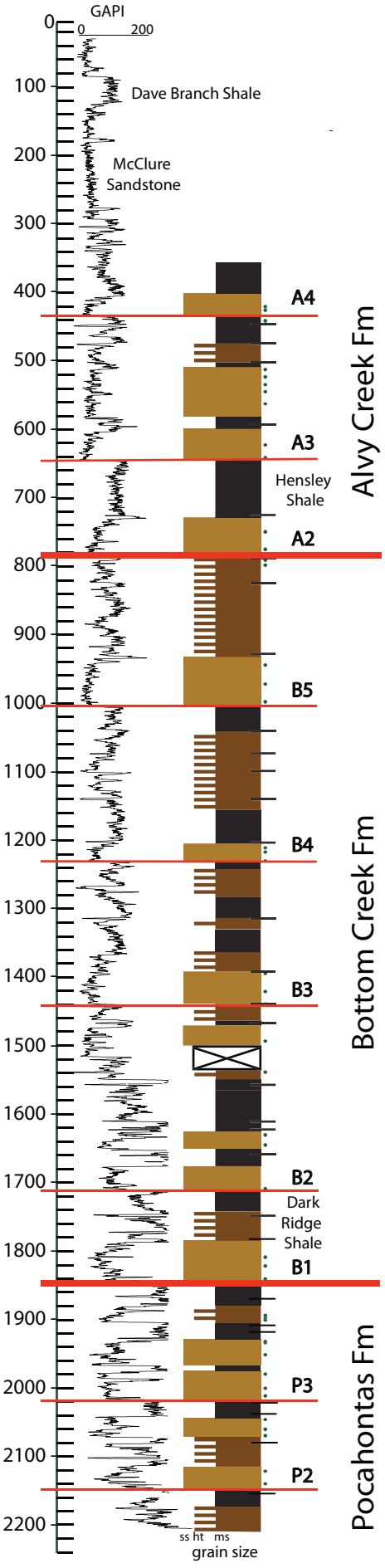

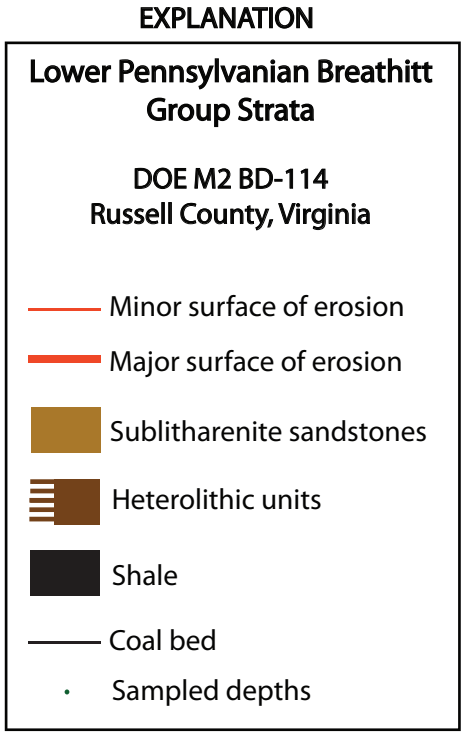

Figure 4: Gamma ray and corresponding lithologies for the M2 core, BD-114. Lithologies grouped into four categories: sandstone, shale, heterolithic units, or coal. Detailed lithologic data collected by Ryan Grimm as part of unpublished description for VCCER Task 2 project. Green circles mark the depths of collected samples in this study.

These units are difficult to differentiate by gamma ray signature, and so are lumped together for correlation purposes.

Mudstones: These vary in color from black to medium gray. There are several regions with thick mudstone and shale units extending up to 120 m in thickness.

Thick coals: These were redacted from the core for the initial study by VCCER, and details can be found in several papers on the Task 2 projects by Ripepi (**2009, 2011**). Placeholders along the core denote the thickness of each removed coal unit.

Regional Correlation

Bodek (**2006**) identified a series of bounding discontinuities that are recognized across his study area to the west in Dickenson County, Virginia, along both strike and dip directions. He interpreted these surfaces to bound upward-fining and upward coarsening cycles of interpreted 3^{rd}-order and 4^{th}-order origin. Denning (**2008**) traced these discontinuity surfaces to his study area in western Dickenson and Wise County, Virginia, and Rouse (**2009**) into McDowell County, West Virginia. Grimm (**2010**) synthesized stratigraphic information from all the listed previous studies and recognized the lateral extent of these surfaces across all of Buchanan and Dickenson counties, as well as parts of Tazewell, Russell, Wise counties of Virginia, and then into Wyoming and McDowell counties of West Virginia. The interpretations from previous work of Bodek (**2006**), Denning (**2008**), Rouse (**2009**) and Grimm (**2010**) have been extended onto the small-scale correlations required for this study at Russell County, Virginia.

Within the study area, strata are correlated along two cross-sections, oriented parallel to the structural strike (**Fig. 5**) and dip (**Fig. 6**) of the preserved basin, which intersect at the core location, and extend 12.6 km and 10 km respectively. Four basic lithologies are discriminated for stratigraphic correlation: sandstone with low, blocky gamma ray, heterolithic sandstones with

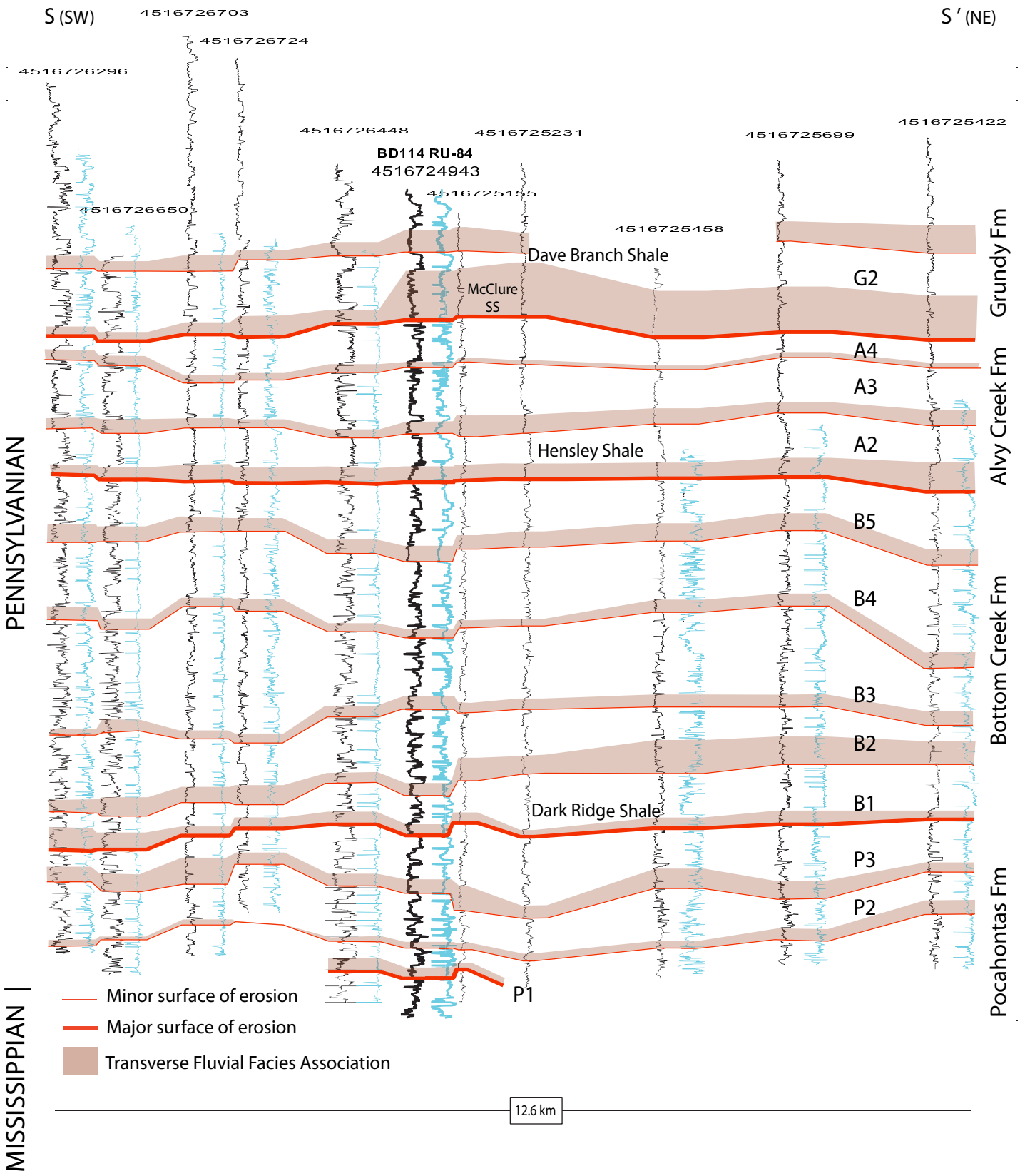

Figure 5: Strike-oriented cross-section. All wells show gamma ray curves in black, and bulk density curves, when available, are in teal. The Hensley Shale is the chronostratigraphic datum across the 12.6 km breadth of the cross-section. Bolded wireline log is the DOE M2 core.

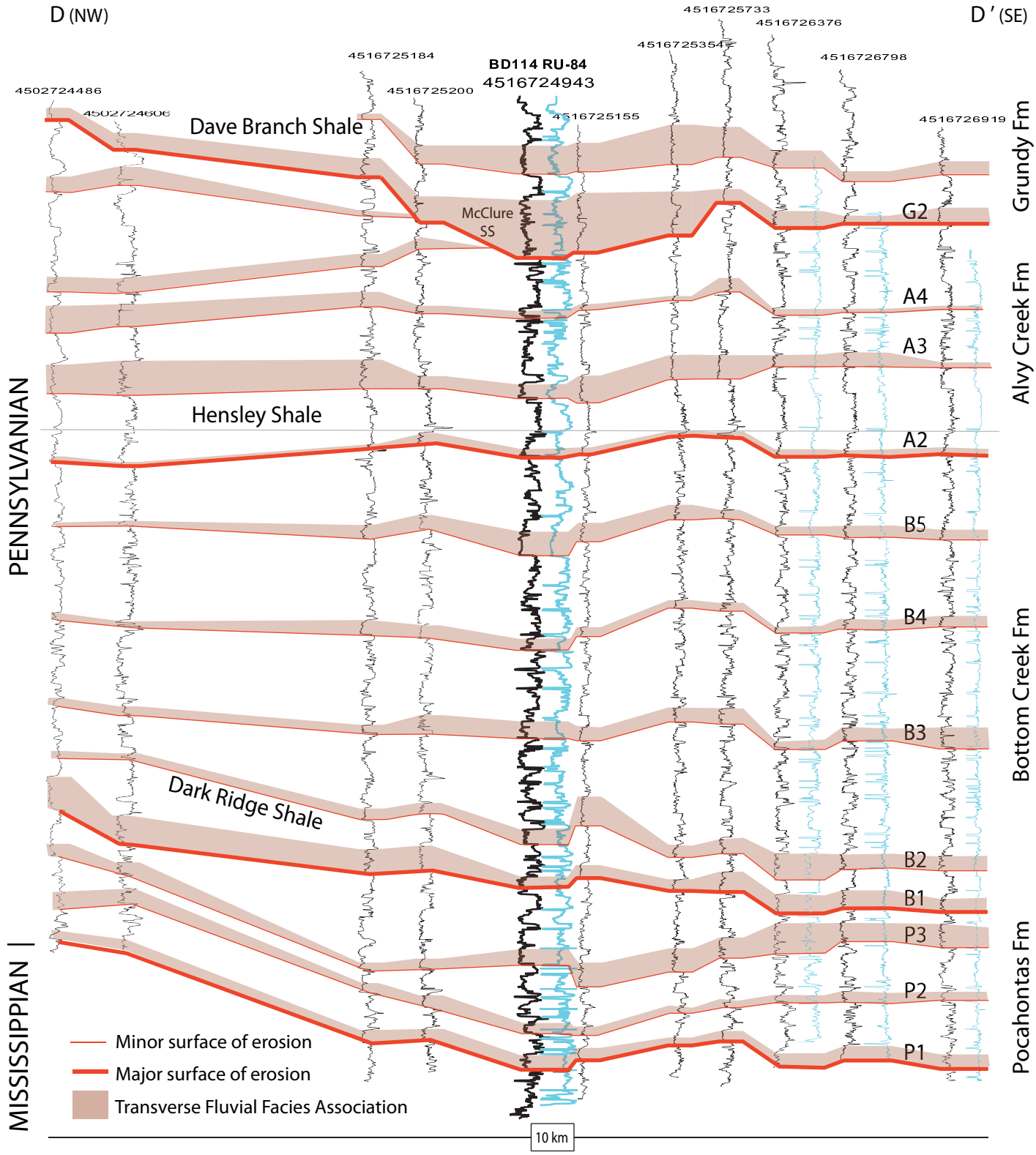

Figure 6: Dip-oriented cross-section. All wells show gamma ray curves in black, and bulk density curves, when available, are in teal. The Hensley Shale is the chronostratigraphic datum across the 10 km breadth of the cross-section. Bolded wireline log is the DOE M2 core.

variable gamma ray, shales with high gamma ray, and coals with low density and high gamma ray. Widespread coal seams present in this region have been used to aid correlation and refine formation picks across the basin.

Major and minor erosional surfaces occur where coal or fine-grained material is sharply overlain by a coarser sandstone unit. Major surfaces of erosion are defined by sharp, distinct gamma ray contacts between sandstone and coal, above traceable patterns in wireline log readings. Minor surfaces of erosion are found between the major surfaces. Major erosional surfaces have thinner fine-grained intervals beneath the discontinuity than those beneath minor erosional surfaces (**Bodek, 2006; Denning, 2008; Rouse, 2009; Grimm 2010**).

These erosional surfaces bound packages of rock that exhibit similar stratal stacking patterns. These packages can be grouped by how often they repeat: high-frequency sequences divided by minor erosional surfaces and low-frequency composite sequences divided by major erosional surfaces.

High-frequency sequences exhibit upward-fining and upward-coarsening trends. In upward-fining successions, basal sandstone bodies grade upward into siltstone and mudstone, capped by a coal unit immediately below the next erosional surface. This fining-upward succession of lithologies has a steadily increasing gamma ray. Upward-coarsening successions begin with a shale that overlies a coal bed, which grades upward into a mixed heterolithic facies. Overall upward-coarsening successions may contain thinner upward-coarsening and upward-fining intervals, which gives the gamma ray signature a bell-shaped curve (**Rouse, 2009**).

Genetic classification of these cyclic packages identifies them as “cyclothems”, coal-bound or “coal-clastic” sequences (**Chesnut, 1994**). The low-frequency composite sequences include three to five high-frequency sequences. A thick, laterally extensive shale unit

immediately overlies the basal sandstone of each low-frequency composite sequence. This shale (e.g. Dave Branch Shale, Hensley Shale, Dark Ridge Shale) is much thicker than most of the sandstone bodies in the sequence.

Lithic sandstone bodies found at the base of the high-frequency sequences are laterally continuous and sub-parallel. These cross-sections are not regional enough to include basin-scale stacking patterns, but the sub-horizontal "layer cake" stratigraphy is recognizable. The dip cross-section shows a gentle thickening or dipping of units toward the southeast. The McClure Sandstone, a part of the Grundy Formation, truncates the upper sequences from the Alvy Creek Formation in a cut-and-fill channel form, only recognizable on the dip cross-section (**Fig. 6**), right at the core site. On the strike cross-section, there is no truncation, but the McClure Sandstone gets substantially thicker to the northeast of the core site. All other sandstone bodies maintain close to a constant thickness, and no additional thickness trends persist through the cross-sections.

Lithologic volumes were calculated using technical software and a grid-like framework of log data extending over the entire study and through the desired depth interval (**Pashin 2001; Rouse, 2009**). For this study, only wells from the two cross-sections are used to estimate unit volume. For the 126 km^2 of map area around the M2 core, unit volume was measured for the continuous sandstones and the thick, "named" shales. Cross-sectional area measured on the dip-section was projected along the distance covered by the strike. Volumes for each continuous sandstone unit are described in **Table 1**. Multiplying by the total well depth, the total volume of all rock beneath the cross-section defined area is 84 km^3. Out of this figure, an estimated 23 km^3 are lithic sandstone bodies, and 14 km^3 are the named shales. The remaining 47 km^3 includes the thinner shales, heterolithic facies, and coal beds.

Table 1: Estimated Volume of Lithologic Units

Lithologic package	(km^3)
G2 basal sand	3.6
Dave Branch Shale	**4.5**
A4 basal sand	1.7
A3 basal sand	3.1
A2 basal sand	0.7
Hensley Shale	**5.5**
B5 basal sand	1.8
B4 basal sand	1.4
B3 basal sand	1.9
B2 basal sand	2.0
B1 basal sand	3.0
Dark Ridge Shale	**4.4**
P3 basal sand	2.4
P2 basal sand	1.6

Depositional Environment and Controls

Lower Pennsylvanian paleoenvironments are discussed in Korus (**2002**), Bodek (**2006**), Denning (**2008**), Rouse (**2009**)**,** and Grimm (**2010**), and the interpretations from these authors have been used on the Russell County core and cross-section data.

The sublitharenite sandstone composition, the paucity of marine fossils and bioturbation, and the stacking pattern of sandstones with heterolithic siltstones, mudstones and coals are consistent with a terrestrial non-marine environment. The grain types, conglomerate lags, and channel-form structures support an immature fluvial depositional setting. The alternation between massive sandstone and fine-grained perturbed beds with coals suggest flooding and ebbing fluvial environments with periods of turbulent and quiet waters. The minor upward-fining sequences have been interpreted as lowstand and transgressive incised-valley fill, alluvial and estuarine deposits (**Allen, 1993; Bodek, 2006; Denning, 2008; Rouse, 2009**), whereas upward-coarsening successions have been interpreted as highstand prograding deltaic deposits (**Korus, 2002; Greb and Martino, 2005; Bodek, 2006; Denning, 2008; Rouse, 2009**). Cross-bedding cosets and lateral accretion sets in the same sandstone bodies in outcrop support a paleoflow to the west and northwest (**Grimm, 2010**).

The transverse fluvial facies association was assigned to these units by Grimm (**2010**). A large-scale braided fluvial system has long been suggested as the depositional environment for the Breathitt Group, with separate source areas for the longitudinal trunk stream, and the perpendicular transverse tributaries (**e.g. Houseknecht, 1980; Archer and Greb, 1995; Bodek, 2006**). The transverse component transported immature sediment from the thrust front, flowing west-northwest into the trunk river flowing southwest (**Davis and Ehrlich, 1974; Graham et al., 1975; Houseknecht, 1980; Korus, 2002; Reed et al., 2005a**).

The low-frequency sequences correspond to each of the Breathitt Group formations (**Fig. 5, 6**), and were assigned based on unit descriptions and gamma ray signatures from the published literature (**Chesnut, 1996; Grimm, 2010**). Above the uppermost major erosional surface is the lower Grundy Formation, below it, the Alvy Creek and Bottom Creek formations respectively, and below the lowermost major erosional surface is the upper Pocahontas Formation (**Fig. 5, 6**). The notable shales and coals of the Breathitt Group were identified along the core. Thirteen high-frequency sequences out of the fifteen identified by Grimm (**2010**) are recognized in the wells along both cross-sections. Age-dated strata (**Fig. 2**) in the lower Pocahontas Formation (318.1 ± 1.3 Ma; **Davydov et al., 2004**) and the upper Grundy Formation (316.1 ± 0.8 Ma; **Lyons et al., 2006**) have been used to estimate average sedimentation rate for these strata. Each high-frequency sequence deposited in about 100 k.y., while the low-frequency composite sequences took 300-500 k.y. to fully develop.

The shorter-term high-frequency sequences are largely governed by glacio-eustatic controls due to short eccentricity-driven Milankovitch cycles of ~100 k.y. duration (**Pashin, 2004; Greb et al., 2008; Grimm, 2010**). Papers that attributed these cycles to 400 k.y. lower-frequency eccentricity (**Chesnut, 1994; Bodek, 2006; Denning, 2008; Rouse, 2009**) use now obsolete timescales. Cecil (**1990**) suggested that high-frequency cyclothems were significantly influenced by climate; increased aridity decreased vegetation promoting run-off and therefore increased sediment supply. His hypothesis is largely inconsistent with climatic data that suggest the region was consistently humid tropical through all stages of sequence development (**Eble, 1996; Reed et al., 2005; Grimm, 2010**). Low-frequency composite sequences have been ascribed to tectonic controls. The wedge-like shape of the composite sequences and the angular truncation of the Breathitt Group by the Lee Formation sandstones suggest a change in

accommodation space most readily attributed to tectonic forces (**Tankard, 1986; Blair and Bilodeau, 1988; Chesnut, 1994; Grimm, 2010**). Evidence for this is not visible in the small-scale cross-sections of this study.

RESULTS - PETROGRAPHY

Framework grains

Grain size, shape and abundance were recorded for framework grains. Abundance ranges listed for each grain type delimit one standard deviation from the calculated mean of each framework grain component. **Table 2** summarizes the framework grains that are present in these samples, and photomicrographs of diagnostic framework grains can be found in **Figure 7**.

Monocrystalline quartz grains: These vary from very-fine to medium grain sized sand. Most are blocky in character, but grain shape ranges from angular shards to rounded sand grains (**Fig. 7a**). Rounded grains are relatively rare, which results in rounded quartz grains within a highly varied assemblage (**Fig. 7b**). Monocrystalline quartz grains exhibit straight to undulose extinction patterns, and several distinct igneous quartz textures were observed: vermiform chlorite inclusions (**Fig. 7a**) and increased vacuolization. Over the core, monocrystalline quartz comprised between 15 and 40 percent of the total grain abundances.

Polycrystalline quartz grains: In this study, all quartz grains with more than one crystal extinction within its grain boundaries were grouped in the polycrystalline quartz grain category (e.g. **Pettijohn, et al., 1972**). Grains exhibiting subequant polygonized, elongate, crenulated, and sutured textures were observed in these samples and indicate a metamorphic source area. Polycrystalline quartz grains signifying different levels of source area deformation are often found in juxtaposition (**Fig. 7c, 7d**). Most polycrystalline quartz grains were angular to sub-angular and very-fine to fine sized. While less durable than monocrystalline quartz, disintegration of polycrystalline quartz grains was not documented in this study. Polycrystalline quartz made up between 18 and 45 percent of the total grain abundances.

Table 2: Compositional Elements Used in Point Counting

I. **Mineral Grains**	II. **Lithic Fragments**	IIIa. **Authigenic replacement minerals**
Quartz Qm – Monocrystalline Qp – Polycrystalline **Feldspar** Fk – Potassium feldspar Fp – Plagioclase **Heavy minerals** Z – Zircon T – Tourmaline	**Metamorphic rock fragments** Lm – Schistose fragments Micas M – Muscovite Bi – Biotite Chl – Chlorite Se – Sericite **Sedimentary rock fragments** Ls – Silt, mud and claystones Ch – Chert IIb. **Intrabasinal components** Organic material Rip-up clasts	Siderite Calcite Kaolinite Chlorite Illite IIIb. **Cements** Calcite Chlorite Siderite Silica

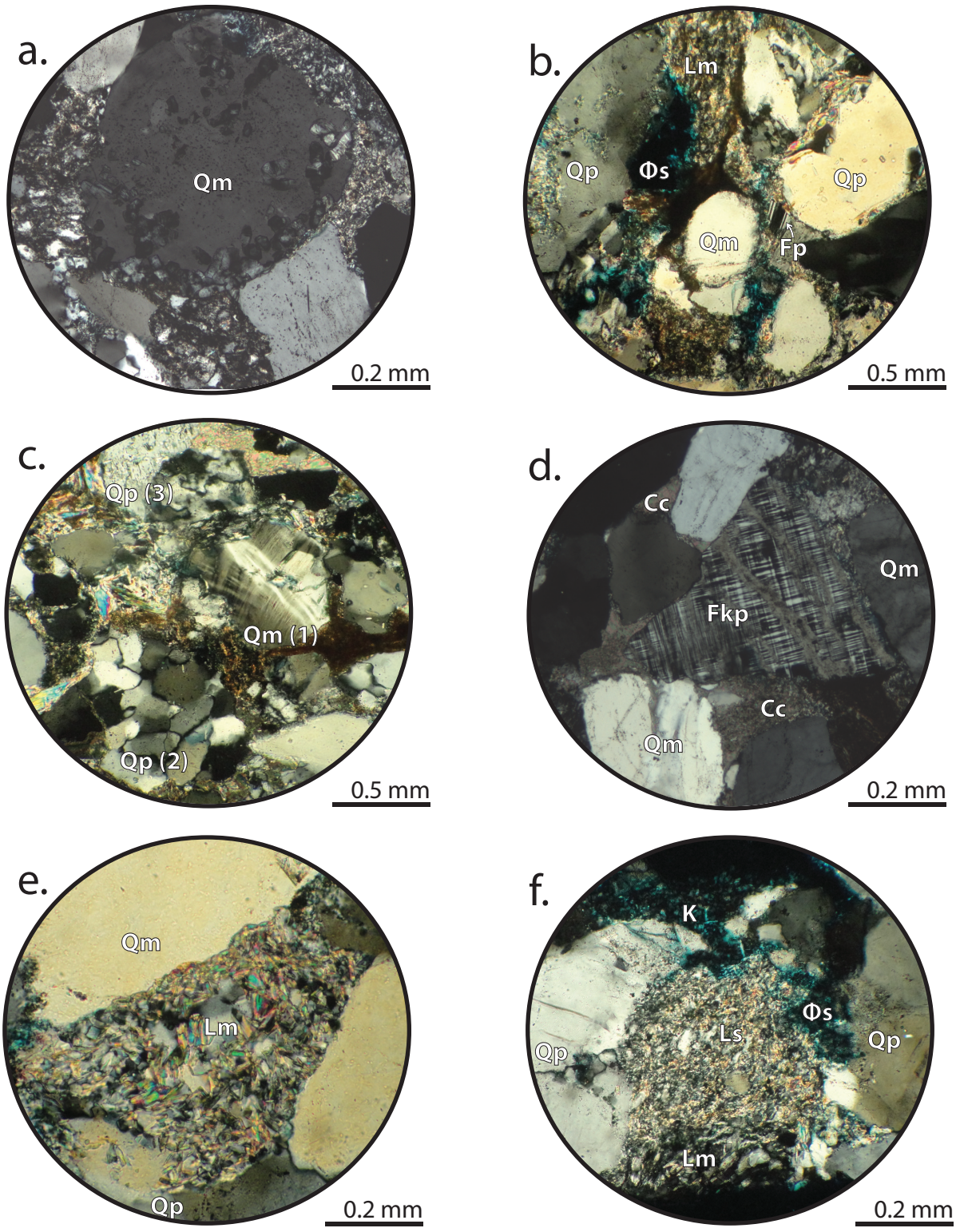

Figure 7: Photomicrographs of Diagnostic Framework Grains. (a) Rounded monocrystalline quartz (Qm) grain with vermiform chlorite inclusions, cross-polarized light; (b) Typical grain assemblage, with rounded monocrystalline quartz (Qm), polycrystalline quartz (Qp), plagioclase feldspar (Fp), metamorphic lithic (Lm), and moldic secondary porosity (**Φ**s) in cross-polarized light; (c) Three different examples of quartz: undulose monocrystalline quartz (Qm(1)), polygonized polycrystalline quartz (Qp2), and crenulated polycrystalline quartz (Qp3), in cross-polarized light; (d) Common perthite (Fkp) grain, host grain is tartan-twinned microcline, while the elongate bleb is plagioclase, surrounded by calcite cement and quartz,

Lithic grains/matrix: These are abundant in the sandstones. For identification purposes, lithic fragments were lumped together into two broad categories: metamorphic lithics and sedimentary lithics, but there was a wide variety of individual compositions. Most abundant were metamorphic fragments, which are largely schistose, with mica grains oriented along a preferred direction: quartz-sericite schist (**Fig. 7e**), quartz-chlorite schist, and micaceous lithic fragments. Sedimentary lithic fragments had greater variability in composition, including mud-and-siltstones (**Fig. 7f**), clays, chert, and siderite nodules (**Fig. 8a**). Intrabasinal components such as sedimentary rip-up clasts and organic debris were abundant, but not included in point-counting percentages because they do not represent recycled material from a distant source area. Many of the mudstone and siltstone grains are visibly illitized. Grain size for lithic grains ranges from very fine to coarse pebble-sized, with the largest clasts sedimentary in origin. All lithic fragments were ductily deformed during burial, forming an abundant pseudomatrix and completely obscuring original grain shape. Lithic grains (not including micas or heavy minerals) comprise 18 to 34 percent of the sampled grains per slide.

Feldspar grains: These have a highly variable mineral abundance. Though mechanically hardy minerals, the relative chemical instability of feldspars when compared with quartz resulted in a decreased presence in the sample set. Feldspars in these rocks were divided into two end-members, based on mineral chemistry: plagioclase and potassium feldspars. Plagioclase often exhibited noticeable twinning in cross-polarized light (**Fig. 7b**), and microcline has cross-hatched tartan twinning. Untwinned potassium feldspar was easily recognized through being highlighted by K-Ferrycyanide staining, differentiating it from untwinned plagioclase. Prevalent secondary alteration and dissolution affected feldspars; plagioclase was commonly replaced by calcite, while potassium feldspar grains were commonly subject to secondary porosity

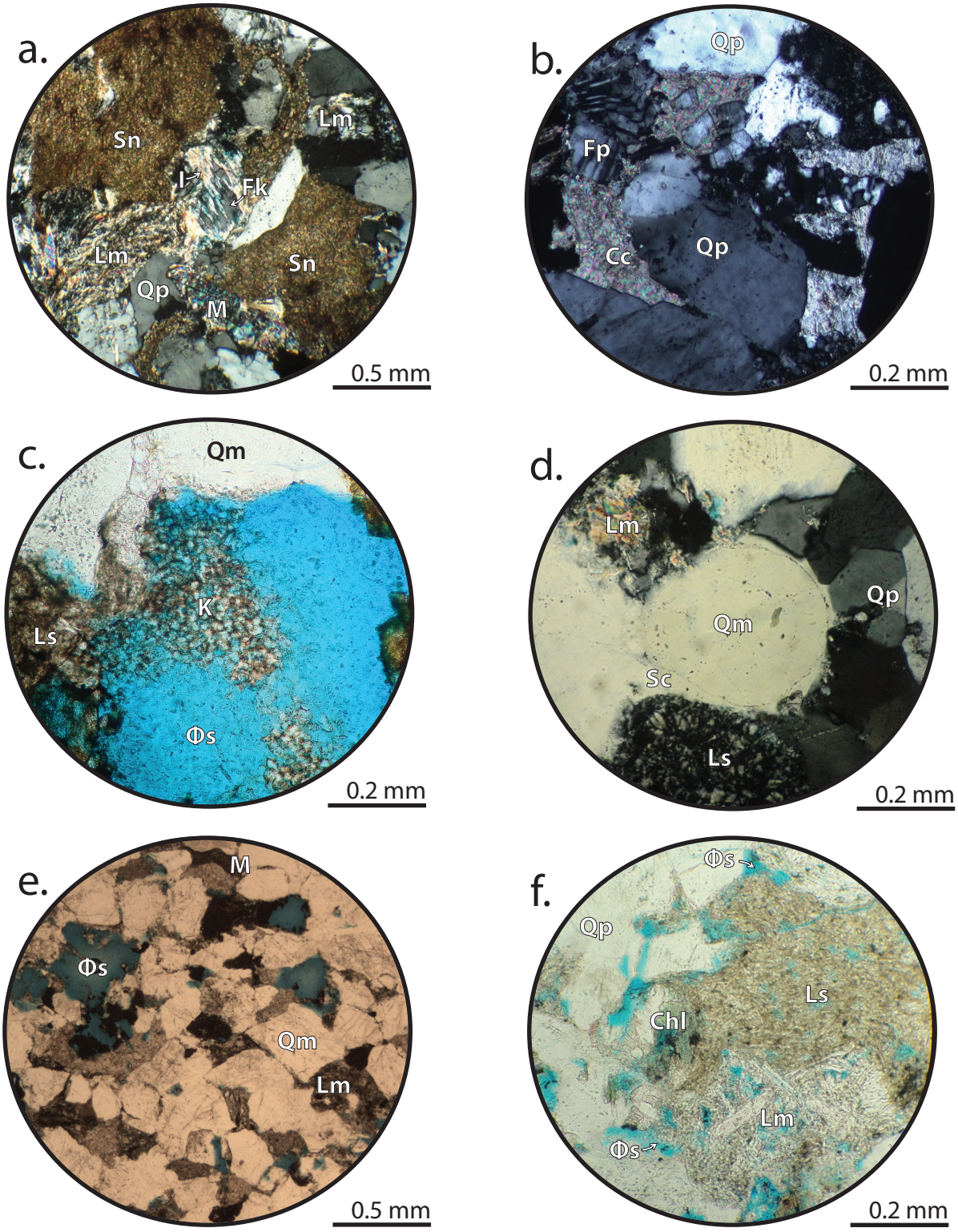

Figure 8: Photomicrographs of Diagnostic Secondary Minerals and Porosity. (a) Siderite nodule (Sn) between metamorphic lithics (Lm), polycrystalline quartz (Qp) and muscovite (M), seen in cross-polarized light; (b) Poikilotopic calcite cement surrounding polycrystalline quartz and plagioclase grains, viewed in cross-polarized light; (c) Large moldic porosity space partially refilled by kaolinite, in plane-polarized light; (d) Silica cement (Sc) as quartz overgrowth around a monocrystalline quartz grain, chert, polycrystalline quartz, viewed in cross-polarized light; (e) Dissolution of framework grains forms moldic secondary porosity in plane-polarized light; (f) Intragranular porosity in lithic fragments in plane-polarized light.

development. Irrespective of mineral chemistry, feldspar grain size varied from very fine to coarse and grain shape ranged from sub-rounded to sub-angular. Plagioclase was more abundant than potassium feldspar. The total feldspar abundance was between 5 and 8 percent of the total grains in the sample set.

Perthite consisting of intergrown plagioclase and potassium feldspar comprised a significant percentage of the feldspar content in some samples. Though perthite forms as a result of both igneous and metamorphic processes, the elongate bleb and flame perthite textures (**Fig. 7d**) most often identified in these samples are related to metamorphic and migmatitic origins (**Walker, 1984; Deer et al., 1997; Vernon, 1999**). Grains with flame perthite structure have 0.1-1 mm long albite intergrowths in the potassium feldspar, oriented sub-parallel irrespective of mineral cleavage, according to the stresses present at formation (**Pryer and Robin, 1996**). Elongate blebs of albite form irregular sizes and shapes in the potassium feldspar host grain (**Deer et al., 1997**). The types of perthitic texture observed in these samples developed in both twinned and untwinned potassium feldspar. These grains were often subject to partial dissolution and intergranular porosity development. Present perthite feldspar grains were counted based on their host grain, potassium feldspar, and not differentiated from potassium feldspars without perthite textures in tabulation.

Accessory minerals: Micas including muscovite, chlorite and biotite, and heavy minerals such as zircon and tourmaline are present as single-mineral detrital grains. For counting and plotting purposes, these grains were included in the *Lithics* category, after Dickinson and Suczek (**1979**). Mica flakes often experienced ductile deformation around more resistant framework grains, based on the mechanical instability inherent to the sheet silicates. Micas retained their flake morphology, without exception, even as they split apart due to mechanical and chemical

deterioration. Resistant accessory minerals, such as zircon or tourmaline were extremely rare in the sample set, and were rounded to sub-rounded when they were present. Micas composed between 2 and 6 percent of the total grain abundance, while heavy minerals composed less than 1 percent.

Authigenic minerals and cements

Pseudomatrix of warped and deformed lithic fragments in this study area influences the composition of cements and authigenic minerals, and distinguishes it from the silica-rich and kaolinite-rich authigenic mineral suites studied to the north and west (**Houseknecht, 1980; Milliken, 2003; Reed et al., 2005**). The pseudomatrix accounts for much of what binds the rock together. Secondary minerals and cement, however, locally comprise up to 24% of mineral components. For each of the major secondary minerals and cement types present in these samples, the observations taken were threefold: depth, morphology, and preferential relationship to specific framework grains. The list that follows describes secondary minerals in decreasing order of abundance.

Siderite: In addition to its presence as an intrabasinal nodule (**Fig. 8a**), siderite is developed as a pore-filling cement, occupying either primary or secondary pore spaces. Both nodular "wheat-seed" siderite as well as its basal, euhedral form were present in these samples, locally even in the same pore-fill. Where siderite is present, it is often pervasive. Siderite occurred near no preferred framework grain; it filled pores near every type of grain identified in this study. Siderite was the most abundant secondary mineral found in this sample set.

Calcite cements and replacements: These were the second most abundant secondary mineral. Calcite fills pore spaces typically with a single crystal of calcite, some exhibiting sweeping extinctions. Euhedral calcite rhombs (associated with high magnesium content (**Folk,**

1974)) and poikilotopic fabric (**Fig. 8b**) are present but rare in these samples. Lithic fragments and plagioclase grains are commonly replaced by calcite. In some samples, calcite cements are subject to secondary porosity development. Scanning electron microprobe and cathodoluminescence analyses supplemented petrographic observations of calcite cement. Calcite cements were examined by SEM for the relative presence of ferrous iron, magnesium, manganese and calcium (**Fig. 9a**). Since the probe does not analyze for carbon dioxide, the stoichiometric percentages of those four cations in oxide form should sum to approximately a 56% value. At five out of the seven analyses of calcite cement, the measured total of the four cations exceeded 56%, likely due to location on the rim of the grain, likely accidental probe overlap with surrounding silicate framework grains. The evaluated calcite was enriched with ferrous iron, but not to the level of ankerite (**Macaulay et al., 1993**). Cathodoluminescence analysis of calcite cements from this same depth showed bright to dull orange luminescence (**Fig. 9a**), associated with the cement's manganese content in the Mg-position (**Richter et al., 2003**). The presence of manganese results in brighter luminescence, while enrichment in ferrous iron is associated with dull luminescence. When the ratio of iron to manganese is less than 10, the percentage of manganese overpowers iron quenching (**Meyers 1974; Bruhn et al., 1995; Budd et al., 2000**). Variations observed in luminescence intensity show changes in manganese abundance relative to ferrous iron during cement development. Continually reducing environments, like deep basinal environments, tend to produce a succession of bright to dull orange luminescences (**Bruhn et al., 1995**). No concentric zoning indicative of multiple generations of calcite cement with varying composition was observed.

Kaolinite: Occurring both as cement and a replacement, kaolinite forms generally after potassium feldspar. However, it is often difficult to determine host grain in the entire

a

Cathodoluminescence imagery of calcite cements

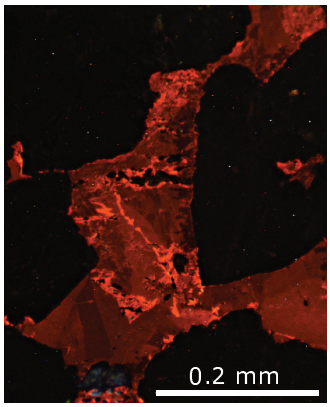

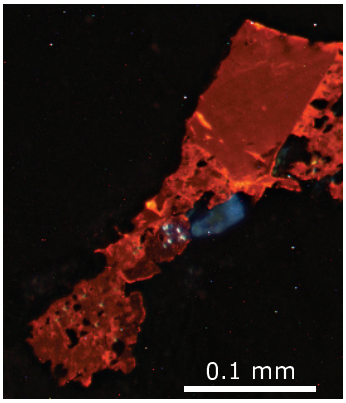

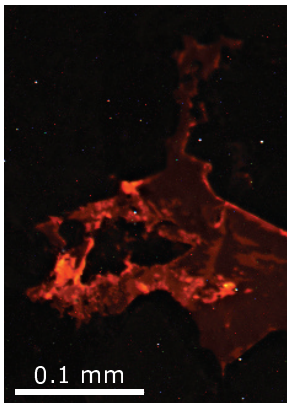

Highest Mn^{2+} content

Lowest Mn^{2+} content

Scanning electron microscopy

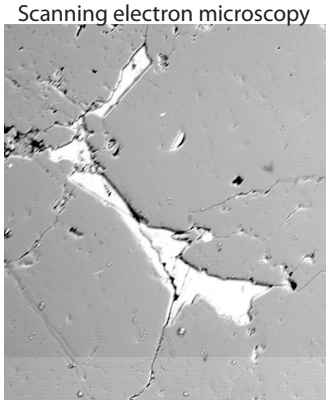

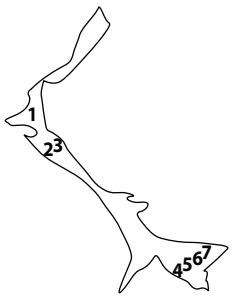

0.2 mm

	MgO	CaO	MnO	FeO	Total(%)	Fe/Mn
1	0.001	55.261	0.632	1.075	56.969	1.7
2	0.142	54.669	0.862	1.397	57.07	1.6
3	0.000	58.242	0.438	0.81	59.49	1.8
4	0.089	52.465	0.508	1.524	54.586	3
5	0.037	57.646	0.551	1.436	59.67	2.6
6	0.069	54.533	0.498	1.309	56.409	2.6
7	0.036	52.381	0.487	1.261	54.165	2.6

b

Light microscopy, cross-polarized light

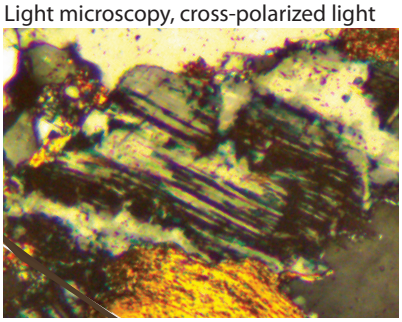

0.2 mm

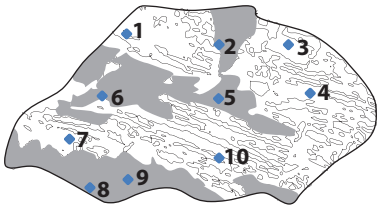

Scanning electron microscopy

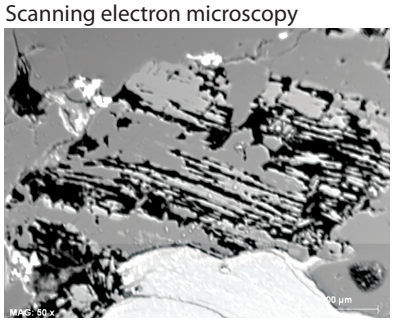

Cathodoluminescence imagery

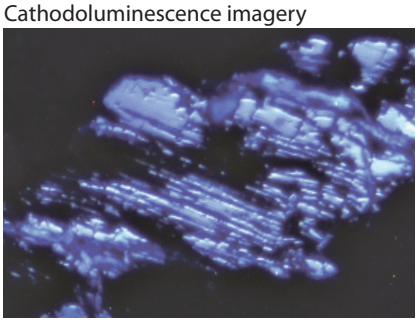

	SiO_2	Al_2O_3	CaO	FeO	Na_2O	K_2O	Norm Wt%	
1	63.33	19.17	0	0.04	0.29	15.86	96.34	orthoclase
2	68.28	19.99	0.14	0.02	11.44	0.16	95.59	albite
3	64.14	18.66	0.04	0	0.62	15.42	93.74	orthoclase
4								empty space
5	68.25	19.84	0.16	0.07	11.15	0.16	94.35	albite
6	68.05	19.68	0.01	0.19	9.66	2.27	81.74	albite
7								empty space
8	67.42	19.62	0.13	0.16	8.32	4.78	67.62	albite
9	69.12	20.03	0.16	0.15	11.23	0.12	95.03	albite
10	61.18	17.7	0.04	0.19	1.66	13.15	80.33	orthoclase

Figure 9: Scanning Electron Microprobe and Cathodoluminescence Photos and Analyses of a) perthitic feldspar and b) calcite cement. Figure combines information from back-scatter electron imaging, light-microscopy, and cathodoluminescence with microprobe elemental analyses.

replacement or complete absence of the framework grain. Kaolinite is better developed in some samples than in others, and there is no evidence of systematic spatial distribution. Kaolinite cement often contains microporosity, elsewhere it only partially filled much larger pore spaces (**Fig. 8c**).

Illite: This occurs as a replacement mineral in this sample set, affecting sedimentary lithics and plagioclase feldspar (**Fig. 8a**). Illite rarely forms as pore-filling cement. Siltstone and mudstone fragments are most susceptible it illite if they have smectite in their original composition. The difference between plagioclase feldspars impacted by sericite and those by illite is difficult to ascertain petrographically. For the purposes of this study, sericitization is categorized with illitization for feldspar alteration.

Silica and chlorite: These are minor cements in the study interval. Chlorite cements occur as grain-rims around small feldspar grains and micaceous lithics. Chlorite is estimated to be an early diagenetic cement because it coats framework grains without being impeded by other authigenic minerals. However, textural evidence does not confirm whether early clay rims converted to chlorite later in diagenesis (**Spötl et al., 1994**). Though early chlorite grain coatings commonly act as a silica cementation inhibitor, neither cement was common enough to exhibit this relationship. Silica cements form exclusively around silica-rich grains such as rounded monocrystalline quartz or chert (**Fig. 8d**). While pressure solution may be the primary source of aqueous silica in quartz arenites (**Sibley and Blatt 1976; Houseknecht, 1984; Houseknecht 1988; McBride 1989; Bjorkum, 1996**), the silica cement in these lithic arenites separated by mud and shale may have been sourced from silica-releasing reactions, like the illite-smectite conversion, common to shale diagenesis (**McBride 1989**).

Albitization: This was noted replacing regions within potassium feldspars. Albite was not observed forming pore-filling cement or extending beyond the edges of the (former) potassium feldspar grain. In order to distinguish albitized grains from igneous or metamorphic albite, four diagnostic characteristics were identified for the samples in question after Saigal et al. (**1988**) and Kastner and Siever (**1979**) using light microscopy supplemented by scanning electron microprobe and cathodoluminescence analyses (**Fig. 9b**). Diagenetic albite is characterized as untwinned, euhedral crystals of the sodic feldspar, which would not have remained intact if subjected to transport and dissolution processes. This morphology distinguishes albitized feldspar from sub-parallel oriented blebs or flame structure albite exsolution in perthite grains. Diagenetic albite also is more compositionally pure (≥95%Ab) than its igneous and metamorphic counterparts. Elemental substitutions in the albite structure are limited by availability and the low temperatures at which albitization occurs (**Kastner 1971; Saigal et al., 1988**). The anomalously low %Ab values for sites 6 and 8 likely suggests that the electron beam captured some host material due to their location on the edge of the grain. Authigenic feldspars lack cathodoluminescence, due to the absence of manganese and iron activators in the feldspar structure. Unlike igneous and metamorphic feldspars which give bright blue cathodoluminescence, authigenic albite will remain dark (**Kastner and Siever, 1979; Richter et al., 2003**). Finally, authigenic albite contains minute grayish-white inclusions, which are fluid-filled vacuoles, visible to a petrographic microscope (**Saigal et al., 1988; Kang-Min et al., 1997**). Since these four criteria were recognized in the perthitic feldspars, it is concluded that they are of diagenetic origin.

Porosity and permeability

No primary porosity was identified in this study, due to the abundance of ductile lithic grains that deformed when compacted. Secondary porosity ranges from 2 – 9%. Generally, units with fewer lithic components and more monocrystalline quartz had the largest porosity values. Secondary porosity was identified in four forms: microporosity, moldic porosity, intergranular porosity and intragranular porosity. Microporosity was most common between crystals of kaolinite pore-fill. Moldic porosity typically occurs at the expense of feldspar grains (**Fig. 8e**), or at the expense of unstable grains in lithic-dominated assemblages. Intragranular porosity is most common within potassium feldspar grains. Intergranular porosity is most common within lithic fragments (**Fig. 8f**) or an unstable secondary mineral such as a calcite or illite.

Since secondary porosity depends greatly on location and availability of unstable framework grains, matrix and cement, the connectedness of created pore spaces is uncertain. This study did not investigate porosity in three dimensions or evaluate permeability of the sandstone bodies. Permeability of similar Pennsylvanian units from Dickenson County, VA, was evaluated by Grimm (**2010**). At depths 900 and 1963 feet below the surface with confining pressures of 800 psi, medium-coarse sublitharenites were reported to have 4.6 nanodarcys and 9.2 nanodarcys of permeability respectively. While exhibiting a broader range of permeability than the finer-grained lithologies, the sandstones still have relatively low permeabilites (0.005-0.008mD).

Mineral abundance trends

The sandstones evaluated in this study vary in compositional abundance of quartz, feldspar and lithic components, but all samples plot as sub-lithic and lithic arenites. According to the QFL plot after Dickinson (**1985**), lithic and sublithic arenites fall into the category of

recycled orogenic provenance (**Fig. 10a**). There is little scatter in the data; almost all of the data fit inside this provenance region. When the mineral abundance data is reorganized to group all metamorphic-sourced quartz into the lithics component, the provenance assessment is more specific: recycled lithics and recycled transitional debris (**Fig. 10b**). This categorization of the data shows more specifically the ratio between igneous and metamorphic components: a significant portion of the total quartz is metamorphic. Evidence for lithic-rich recycled sediment and transitional-to-quartzose recycled materials mixing at deposition in the study area is consistent with the transverse stream component of paleoenvironmental models proposed by Grimm (**2010**) and Bodek (**2006**).

Primary and secondary mineralogy change in relative abundance over the core depth. The sample collection density, the heterogeneity of diagenetic products (**Milliken, 2003**), and the heterolithic nature of the stratigraphy lend itself to a changing sandstone compositional character with depth (**Fig. 11**). However, present depth is a minor control on any observable trends, given the short core and that the Appalachian basin is no longer subsiding. Additionally, the stratigraphic interval intersected by the DOE M2 core has thicker, more distinct sandstone bodies at the shallower depths which gradually become thinner and more separate sandstone bodies toward the bottom. Proximity to less permeable lithologies with less stable mineralogies and high gamma ray values subject the deeper sandstone units to different pore fluids than the thicker, shallower units (**Curtis, 1978; McBride, 1989**). This has an effect on the types of dissolution and authigenic mineral formation that can occur, and is a dominant control on the observed trends.

Variation in sandstone framework grain abundances was limited over the entire core. Feldspar abundance decreases with depth, with potassium feldspar notably declining in

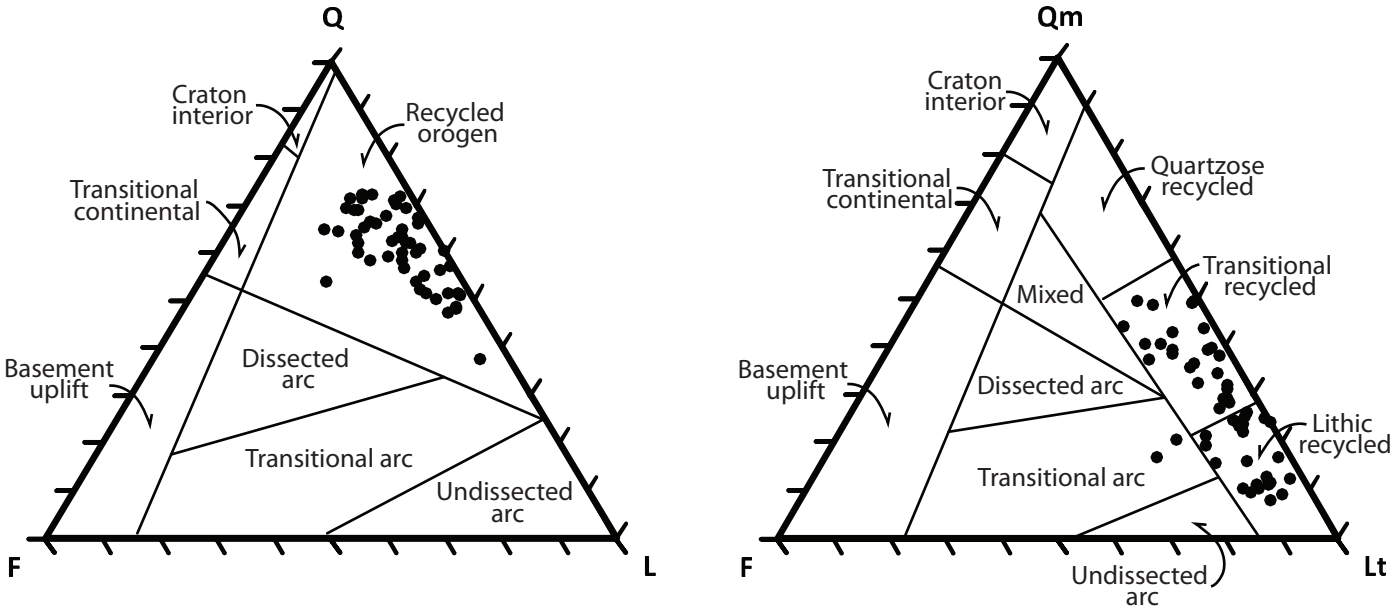

Figure 10: Ternary QFL and QmFLt diagrams. Triplots generated after Graham and Midgley (2000) and internal divisions after Dickinson (1985).

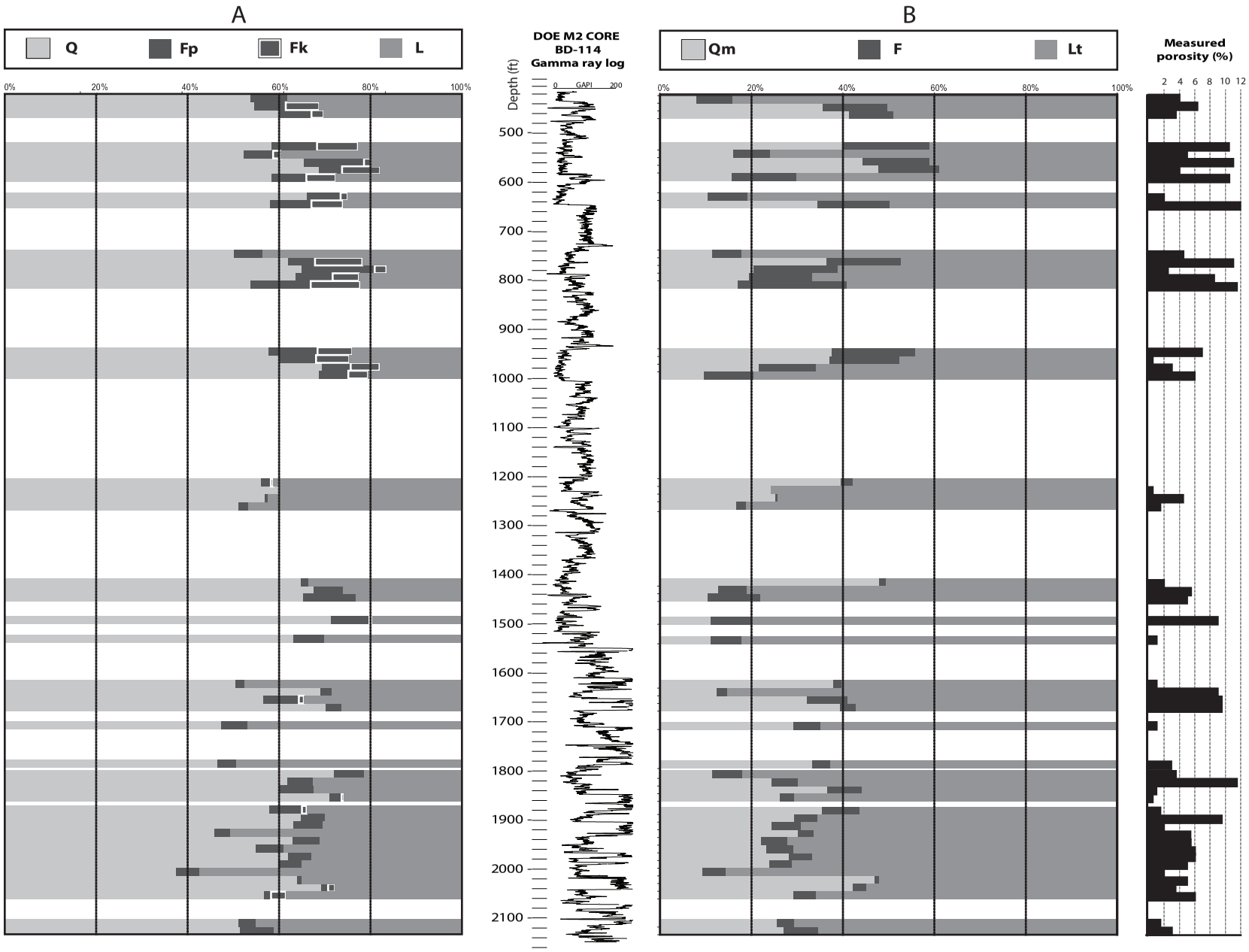

Figure 11: Mineralogy and Porosity Trends with Depth. Gamma ray wireline log in center shows the continuous depth profile. Horizontal bar diagrams showing mineralogical percentages of A) Q: Total quartz, Fk: potassium feldspar, Fp: plagioclase feldspar, L: Lithic fragments; B) Qm: Monocrystalline quartz, F: Feldspars. Lt: Total lithic material including polycrystalline quartz. Porosity measured through point counting for each sample is shown on the far right, also scaled to depth.

abundance below 1000 ft (**Fig. 11a**). Albitization, illitization and moldic porosity at the expense of feldspar grains increases deeper than 1000 ft, indicating that the lower half of the core has experienced more feldspar alteration than the upper section. The QmFLt-to-depth diagram (**Fig. 11b**), shows a general decreasing trend in the quartz-lithic ratio from the top to bottom sample collected within each sandstone body.

On the basis of available data, authigenic minerals and cements exhibited noticeable trends. Silica cementation increases in abundance with depth over the entire core, and, while minor in abundance, is most prevalent in samples from sandstones near a contact with shale or similar high gamma ray lithology. On a smaller scale, siderite cement increases in abundance with depth within each major sandstone body. Calcite cement exhibits that same increasing trend less consistently.

There is no significant correlation between porosity and depth (**Fig. 11**), cement abundance, or rigid framework grain abundance. Only proximity of the measured sample to greater gamma ray values and thinner sandstone bodies results in a lowered porosity.

Paragenesis

The culmination of all the petrography work is the paragenesis (**Fig. 12**), which is the chronological order of secondary authigenic mineral emplacement and development. Textural relationships were derived from light-microscopy whereas geochemical reactions were evaluated based on kinetic and thermodynamic boundary conditions in the published literature. Framework grain composition is the foremost control on what minerals are in the paragenesis, and theoretical modeling has been used to resolve issues of volume, transport, time and distance with respect to possible secondary mineral replacement and formation (e.g. **Aagaard et al., 1990; Morad, 1990; Bjorlykke and Egeberg, 1993; Reed et al., 2005a**).

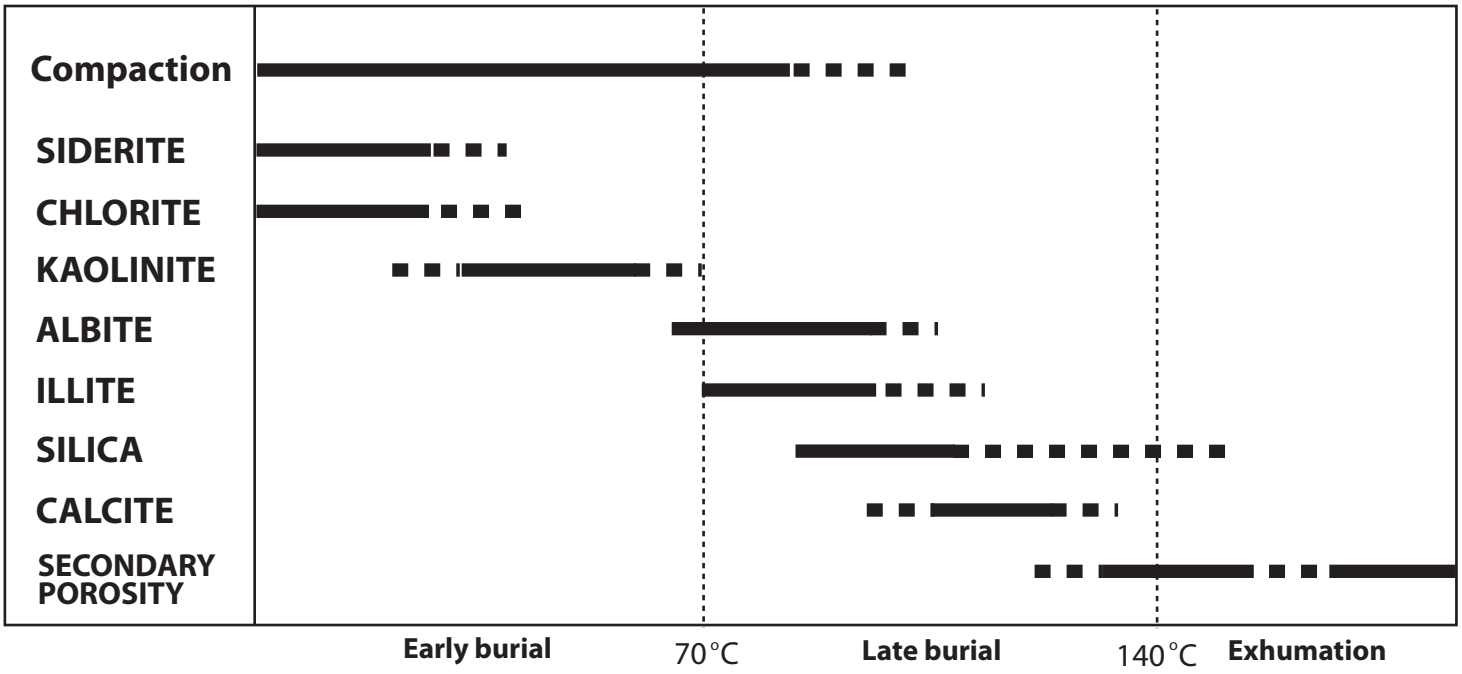

Figure 12: Paragenetic Chart. Secondary minerals are post-depositional, and developed during burial and exhumation. Paragenetic relationships are supported by textural evidence and geochemical considerations. Dotted lines indicate uncertainty. Boundary temperature between early and late burial is based on a threshold value set by Morad, 2000. The boundary temperature between late burial and exhumation was determined experimentally by Reed et al., 2005.

Lower Pennsylvanian sandstones record a broad suite of eogenetic, mesogenetic, and potentially telogenetic reactions. Boundary temperature and pressure conditions used for the three stages of paragenesis are after Morad (**2000**): maximum eogenesis is <70 ^{o}C and <2 km, and mesogenesis occurs at temperatures and pressure above this until maximum burial. Compaction began just after deposition, and continued throughout the burial process. The earliest diagenetic reactions have the most profound effect on the resulting porosity and permeability of the sandstone body (**Curtis, 1978**).

Early Burial

Siderite and chlorite are in contact with primary grain surfaces in rims or coats, and denote the earliest diagenetic events. Siderite is the most prevalent cement in the sample set, and indicates a reducing pore fluid environment in the early stages of compaction (**Fig. 13a**) (**Reed et al., 2005a, b**). Minor proportions of chlorite rims place it at the beginning of eogenesis **(Fig. 13b)**. These units experienced substantial compaction in early stages, deforming labile framework grains into pore spaces and destroying any remaining primary porosity and permeability. Without sufficient fluid pathways, further cementation slowed or halted due to a lack of available pore volume. Kaolinite development depends on the interaction between acidic meteoric waters with feldspar grains (**Lanson et al., 2002**), meaning that it would likely form at shallow burial depths early in diagenesis. Milliken (**2003**) suggested advective transport of aluminum necessary to make kaolinite in the Breathitt Formation. The kaolinite either actively replaced potassium feldspar, or it filled void pore space (**Fig. 12**).

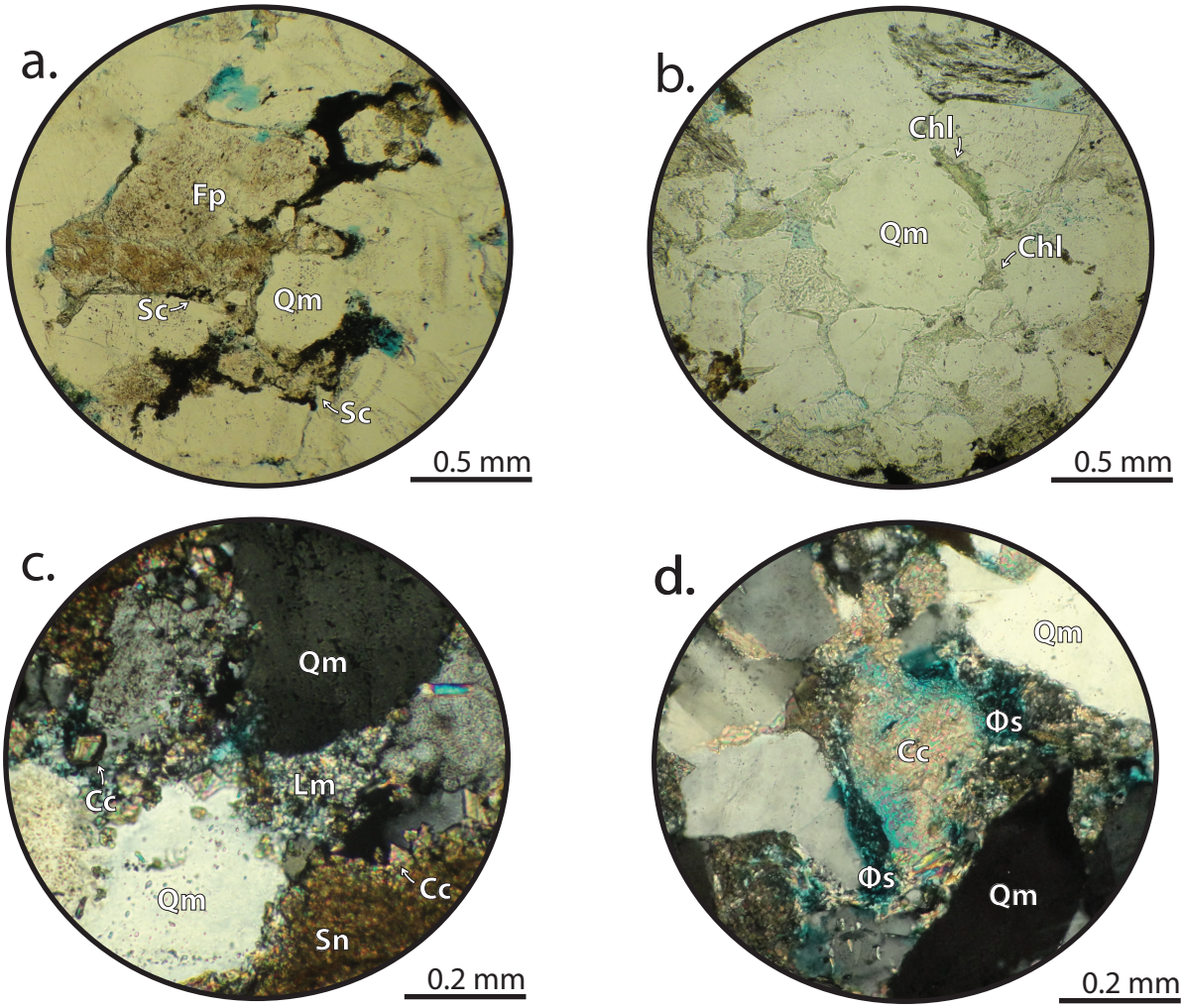

Figure 13: Photomicrographs of authigenic mineral relationships. (a) Siderite cement (Sc) between a plagioclase (Fp) and a quartz(Qm) grain, plane polarized light; (b) Chlorite (Chl) rims on a monocrystalline quartz (Qm) grain, plane polarized light; (c) Euhedral calcite cement (Cc) between two monocrystalline quartz (Qm)grains, a metamorphic rock fragment (Lm)and an intrabasinal siderite nodule(Sn); (d) Secondary porosity at the expense of calcite cement (Cc).

Deep Burial

The temperatures necessary for the onset of albitization have been posited by a number of studies, ranging from as low as 60 ^{o}C in the presence of low pCO_2 (**Saigal et al., 1988; Baccar et al., 1993**) to 120-150 ^{o}C (**Kang-Min et al., 1997; Baccar et al., 1993**) as the threshold of the albite stability field. Since albitization could not take place if calcite cements were in place, filling available pores (**Kastner and Siever, 1979; Saigal et al., 1988; Ramseyer et al., 1992**), no eogenetic calcite cement is likely to have formed and remained prior to albitization.

It is difficult to constrain the relative timing of illitization with only textural evidence. Illitization of smectites in adjacent mudstones can occur contemporaneously with albitization, with the estimated onset at 70-80 ^{o}C (**Aagaard et al., 1990; Baccar et al., 1993**), near the low end of the albitization range. However, illitization of smectites in sedimentary lithic materials can take place irrespective of albitization of feldspar grains. To alter feldspars and kaolinites, illitization requires higher temperatures, above 125 ^{o}C (**Aagaard et al., 1990**). However, temperatures as low as 90 ^{o}C have also been inferred from these units for the onset of illitization, which showed illitization of potassium feldspars being much more widespread than albitization (**Ehrenberg et al., 1993**).

There is little silica cement in these rocks due to the sediment composition and destruction of primary pore space by compaction prior to silica transport. The silica mobility window opens at about ~100 ^{o}C (**Byorlykke and Egeberg, 1993**), which is near the maximum temperature reached by these strata. Reed (**2003; et al., 2005b**) studied fluid inclusions of silica cements farther northeast, and found that a warm silica-rich fluid was injected into the Upper Pennsylvanian Breathitt Formation during Alleghanian thrusting. This silica precipitation and cementation was caused by advective flow through the Upper Pennsylvanian sandstone units.

While the Lower Pennsylvanian sandstones in southwest Virginia do not contain abundant silica cements to support warm fluid injection, advective flow can be inferred as the mechanism silica transport (**Reed, 2003**). Though it began near the maximum burial, silica cementation likely continued during cooling and exhumation due to the inverse relationship between silica solubility and temperature (**Langmuir, 1997**).

Development of a late stage calcite cementation is supported by the enhanced ferrous iron and manganese in the calcite structure measured by SEM. An increased concentration of ferrous iron, magnesium and manganese is consistent with the low redox composition of deep brines present during calcite precipitation (**Langmuir, 1997**). Calcite can be pervasive as cement and a replacement mineral, filling in many secondary pores and replacing pseudomatrix, occasionally forming poikilotopic textures or euhedral crystals (**Fig. 13c**).

Since the maximum burial achieved only about 4.4 km and 140 ^{o}C (**Blackmer, 1994; Hulver, 1997; Reed, 2003; Reed et al., 2005b, and references therein**), and all metamorphic grains and fragments express random degrees and orientations or schistosity, no metamorphism took place on these strata. Metamorphic materials must have experienced deformation prior to transport and deposition. There is no textural evidence to support in situ metamorphism either in the framework grains, matrix or cements qualitatively and quantitatively assessed.

Telogenesis

Using both thermochronologic and paleothermometric constraints, Reed et al. (**2005b**) calculated that the exhumation of the Pennsylvanian units occurred in three stages over about 270 Ma. The first stage, constrained by fluid inclusion and apatite fission track analyses, lasted about 130 m.y. and the Lower Pennsylvanian strata rose about 10m/m.y. The second stage, constrained by (U-Th)/He analyses, was the steepest, rising 1.4 km at a rate of 30m/m.y. The

final stage of exhumation raised the strata 2.1 km to its present location, at a rate of 10 m/m.y. In southwest Virginia, the study interval is still more than 400 ft underground.

It is difficult to texturally identify telogenetic effects. Infiltration of meteoric water may have intensified reactions that started during eogenesis or mesogenesis, which are now impossible to differentiate (**Morad, 2000**). Secondary porosity persists to the present, with dissolution of late stage calcite cements (**Fig. 13d**), indicating that enhancement of secondary porosity took place sometime during exhumation.

LITERATURE REVIEW – GEOLOGICAL CO_2 STORAGE AND SEQUESTRATION

Geological carbon sequestration and storage techniques have developed over recent years to combat increasing atmospheric accumulation of carbon dioxide. As the second most abundant greenhouse gas, carbon dioxide has reached a current level of 394 ppm in the atmosphere (as of May 2011, **Tans and Keeling, 2011**), and its recent increase is generally considered a significant contributor to enhanced global warming and ocean acidification (**Alley et al., 2007**). Since the lithosphere is the largest natural sink in the carbon cycle, with the longest residence time (**Andrews et al., 2004**), geological storage and sequestration has been the subject of much modeling, testing and review as a long-term repository for carbon dioxide. In this process, carbon dioxide is captured directly from its large-scale anthropogenic source, purified, pressurized, and injected into geological media, either permanently (sequestration) or for geologically significant periods of time (storage) (**Bachu and Adams, 2003**). Deep saline aquifers, more than depleted hydrocarbon reservoirs or coal beds, have a great potential capacity for sequestration and storage due to their individual permeability and widespread global occurrence (**Michael et al., 2010; Zahid et al., 2011**).

Alongside sequestration and storage efforts are enhanced hydrocarbon extraction efforts (EOR, ECBM), increase hydrocarbon output of a waning reservoir by flushing it with a carbon dioxide fluid. An Enhanced Coal Bed Methane project has been ongoing over the last 5 years in Russell County, Virginia, targeting the Lower Pennsylvanian coals in the Nora and Dunham Fields (**Ripepi, 2009**). Sandstone bodies intercalated with the coals have been assessed as seal units due to their thickness and low permeability (**Ripepi, 2011**), however, their extensive distribution, lateral continuity, and mineral abundances may show a storage potential for these units. Evaluating the carbon sequestration reservoir potential of these Lower Pennsylvanian sandstone bodies requires background knowledge on modes of geological storage available and

recent trials of carbon sequestration in analogous reservoirs. This chapter reviews the recent published literature to assess the applicability of carbon sequestration to the study interval sandstones.

Modes of Geological Carbon Sequestration and Storage

Upon injection into a potential reservoir, carbon dioxide is initially immiscible with formation waters. Through continued contact with the water and reservoir rock, carbon dioxide will end up either separated from the formation waters as a distinct gas phase, held hydrostatically to the reservoir surfaces, dissolved in the brine, or precipitated into a mineral phase (**Michael et al., 2010**). The controls for each type of trapping depend on the geology of the reservoir rock, the fluid dynamics of the formation waters, and water-rock chemical reactions. Within siliciclastic reservoirs, carbon dioxide can be trapped by mechanisms that fall into three broad categories: physical trapping, solution trapping, or mineral trapping (**Bachu and Adams, 2003**). Coal reservoirs preferentially store carbon dioxide adsorbed onto the microporous surfaces of the coal macerals (**Shi et al., 2008; Kurlenya and Serdyukov, 2010**). Each storage or sequestration mode involves different strengths, weaknesses, time spans and volumes. Since they are controlled by the geology and the changing chemistry of the reservoir, these modes are not mutually exclusive.

Physical Trapping

Physical traps are controlled by the bedrock geometry between the porous reservoir and its impermeable seal or cap, which prevents the escape of the injected fluid. Potential carbon sequestration reservoirs must include a physical trap, to keep the injected carbon in contact with formation waters and reservoir mineralogy long enough for chemical reactions to take place and

impede the release of the gas into groundwater aquifers or back into the atmosphere (**Xu et al., 2006**). The necessary seal can have been emplaced through deposition, as the result of a fault structure, or in relation to salt tectonics (**Bachu and Adams, 2003**). Physical traps are effective in storing carbon dioxide immediately, and can trap over a significant areal extent and volume (**Bradshaw et al., 2007**). Stratigraphic and structural trapping are types of physical traps, and are commonly associated with the accumulation of migrating hydrocarbons (**Biddle and Wielchowsky, 1994**).

The impermeability of the reservoir seal is the greatest control on the integrity of the reservoir. The strength of the seal is the amount of pressure it can withstand before giving way, and therefore the possible volume the reservoir can contain. If compromised, the pressurized carbon not in a mineral phase could release into stratigraphically higher units, shallow groundwater aquifers, or back into the atmosphere (**Lu et al., 2009**). Deep saline aquifers, exhausted hydrocarbon reservoirs and coal seams have been used for carbon sequestration and storage reservoirs where the overburden is thick and impervious enough to prevent the escape of the gas back into the atmosphere.

Pressures at injection depth dictate the volume of the injected carbon dioxide. Deep reservoirs are often selected to maintain the volume conditions of supercritical carbon dioxide. The supercritical phase of carbon dioxide persists at temperatures and pressures in excess of 7.38 MPa and 31.1 ^{o}C (**Fig. 15**) (**Diamond and Akinfiev, 2003**). Temperatures and pressures present at depths greater than 800 m approximate the lowest conditions for supercritical carbon dioxide.

Solubility Trapping

Solubility of carbon dioxide into water is increased at increasing pressures (**Diamond and Akinfiev, 2003**). When the injected carbon dioxide dissolves into the formation waters, it

forms carbonic acid, which then disassociates into bicarbonate, then to carbonate, the kinetics of which depend on pH levels in the brine. These ion contributions then react to form a wide range of mineral salts, depending on the available cations in solution. Solubility trapping is effective on a timescale of hundreds to thousands of years over a basin-scale areal extent; the faster the migration of the carbon dioxide through the reservoir, the less time it takes to dissolve (**Bradshaw et al., 2007**).

Reservoir mineralogy and chemistry are major controls on the fluid composition and pH before, after and during carbon dioxide dissolution. Sedimentary basin strata rich in alkali feldspars have the capacity to buffer pH, since the reactions with its cations do not produce carbonates, but just uptake H+, and therefore they enhance carbon dioxide storage through solubility trapping (**Gunter et al., 2000; Matter and Kelemen, 2009**). Basic silicate minerals, those highest on Bowen's Reaction series, contribute the greatest amount of cations, which can intensify mineralization (**Matter and Kelemen, 2005**).

Formation water chemistry regulates solution trapping stability and longevity. Solubility of carbon dioxide decreases as temperature and ionic strength increase. Conversely, CO_2 solubility increases with increasing pressure (**Portier and Rochelle, 2005**). The carbon-oxide phase trapped in solution can be released if the pressure or formation water chemistry changes, driving the reactions toward precipitation or gas production. On those grounds, solubility trapping is often considered only a temporary storage location (**Bachu and Adams, 2003**). However, analog studies of natural gas fields suggest that solubility trapping is the dominant sink for carbon dioxide in a reservoir over the geologic timescales (**Gilfillan et al., 2009**).

Partial dissolution of carbon dioxide into the formation brines is another means of solubility trapping. Residual trapping separates carbon dioxide into pore spaces cut off from the

larger carbon dioxide plume bound by a layer of immiscible formation water. Capillary pressure prevents further mixing or migration of the trapped carbon dioxide (**Kumar et al., 2005; Qi et al., 2009**). This form of solubility trapping is less dependent on an impermeable seal unit and more dependent on the capillary pressure and available pore space. Residual trapping can occur in hydrocarbon reservoirs as well: removing residually trapped hydrocarbons can be achieved by EOR and ECBM projects (**White et al., 2005**).

Hydrodynamic trapping is also associated with partial solubility trapping, in which carbon dioxide is injected into a deep aquifer with a low flow velocity (**Bachu et al., 1994; Bachu and Adams, 2003**). The trapping mechanism depends on the slow velocity of the plume, limiting contact between the immiscible phases of supercritical carbon dioxide and the formation brines (**Bachu et al., 1994; Gunter, 2000**). An angular contact may result between the immiscible phases due to the flow regime (**Biddle and Wielchowsky, 1994**). When dissolution does occur, the long residence time of plume migration through the aquifer is ideal for slow kinetic reactions in certain mineral formation (**Gunter, 2000**).

Mineral Trapping

Mineral trapping follows solubility trapping, and it is the more stable and permanent sequestration of carbon when it takes effect (**Hellevang et al., 2005**). Divalent cations such as ferrous iron, magnesium, or manganese in solution are produced by dissolution or replacement reactions between the formation waters and the silicate framework grains. Disassociated carbonate ions react with these cations to form carbonate minerals, most commonly calcite, dolomite and siderite (e.g. **Langmuir, 1997; Matter and Kelemen, 2009**). Mineral carbonation traps carbon dioxide on a timescale of tens to thousands of years, over basin-scale volumes (**Bradshaw et al., 2007**).

The carbonate precipitate which forms out of solution varies based on geology and chemistry of the formation waters. Lowering of pH drives dissolution and transformation reactions of silicate minerals:

$$\text{e.g. } CaAl_2Si_2O_{8(plagioclase)} + 2H^+ + H_2O = Ca^{2+} + Al_2Si_2O_5(OH)_{4(kaolinite)}$$

More dissolved silicate minerals from the reservoir results in more pH buffering which enhances both solubility trapping and mineral storage (**Matter and Kelemen, 2009**). A pH decrease induces silica dissolution rates, resulting in a greater silica concentration in the brine (**Kaszuba et al., 2005**). When sodium is supplied by oligoclase dissolution, a major trapping mineral is dawsonite, and when ferrous iron is supplied by chlorite and hematite dissolution, siderite and ankerite precipitate (**Xu et al., 2005**). Reactive formation of siderite at shale-sandstone boundary to the reservoir suggests that shale is the reactive component in the system (**Kaszuba et al., 2005**). Therefore, dissolution of injected carbon dioxide into formation waters is dependent on pH buffering as well as temperature, pressure and geology.

The apparent permanency of carbon immobilization by mineral trapping mechanism contributes to its long-term sequestration, but mineral trapping may also introduce storage safety and longevity problems (**Hellevang et al., 2005**). Carbonate minerals that form as a rim on the surface of a framework grain prevent it from coming into contact with the formation water and contributing cations to solution (**Tenthorey et al., 1998**). Carbonate minerals forming around a carbon dioxide injection site could fill porosity and permeability, impeding the flow of injection and substantially decreasing available reservoir volume. Others suggest that rapid carbonate mineral formation could cause localized fracturing and thereby increased permeability (**Scherer, 1999**).

Basinal brines are characterized by increased ferrous iron, magnesium and manganese levels, proportionate to the amount of time the formation waters have been in contact with the reservoir mineralogies and its inherent flow velocities (**Ennis-King and Paterson, 2007**). However, sedimentary mineralogies in foreland basin fills (quartz, feldspars, micas) do not typically include the weakest silicate mineralogies (olivine, pyroxenes), which most readily surrender them into solution. Accounting for immediate sourcing of chemical elements alone, the cation concentration is too low for widespread and total mineral carbonation (**Dickinson and Suczek, 1979; Xu et al., 2005**). When including the potential of element introduction through convective or advective flow, more mineralization becomes possible (**Ennis-King and Paterson, 2007**). In timescales exceeding 1000 yr, mineral formation may only account for as much as 18% of the total carbon storage in the aquifer (using a natural reservoir analog, **Gilfillan et al., 2009**).

Adsorption

Adsorption is a trapping mechanism for carbon dioxide that is distinct to coal seams, though the other modes are still relevant (**Bustin and Clarkson, 1998**). Coal beds are source rocks, which have in the past and continue to release hydrocarbons as part of its organic maturation, or coalification. Methane, a mature hydrocarbon, is stored in coals as a sorbate, held onto the internal surface of the microporous coals through hydrostatic pressure, which is difficult to displace. Composition and rank do not consistently predict the methane adsorption capacity of a coal bed (**Bustin and Clarkson, 1998**), however a range of 282 – 688 cubic feet of methane per short ton of coal is retained in depressurized coal beds **(Diamond et al., 1986**). Permeability is a strong control on whether formation fluids can diffuse or be transported. Permeability

depends upon confining pressure; the greater the pressure the less the permeability (**White et al., 2005**).

Carbon dioxide has a greater affinity for coal surfaces than methane, and will sorb onto the surface of the coal and immediately displaces any methane over tens to hundreds of kilometers. At depths from 400-2000 m under typical pressure conditions, coal will adsorb between 2 and 10 times more carbon dioxide than methane (**Bradshaw et al., 2007; Shi et al., 2008**). Flushing depressurized oil and gas reservoirs with fluid carbon dioxide or water will enhance methane production by releasing it from its bound state. Carbon dioxide sorption capacity is difficult to predict, but it is very low relative to the physical, mineral and solubility trapping that occurs in saline aquifers (**Bradshaw et al., 2007**).

Recently, enhancing coal bed methane extraction has become an area of research that stores carbon dioxide in the depleted reservoir while also producing methane or oil as a "value-added" process (**White et al., 2005**). Enhanced extraction has the capacity to increase methane flow rates out of gas reservoirs that have become depressurized or poor producers.

Enhanced Coal Bed Methane projects have been in operation in many places across the United States. There is an estimated 400-700 Tcf of gas in the major US coal basins that can be extracted using enhanced recovery methods (**White et al., 2005**). The central Appalachian basin, with its rich coal-bearing strata is no exception. The Pocahontas Basin contains nearly 3.6 Tcf methane which is deemed technically recoverable (**Nolde and Spears, 1998; Lyons, 1998; Milici et al, 2003**).

Increasing carbon storage efficiency

Manipulating the mode of carbon trapping that occurs in a reservoir can either increase of decrease the efficiency of that repository. Any combination of increasing the efficiency of

injection, use of volume, and workable chemistry of reservoirs can increase the efficacy of carbon sequestration and storage.

Testing reservoir permeabilities before injection is essential to the sequestration process. Sodium-bicarbonate enriched waters generally also support high quantities of rare earth elements, which can be used as tracers through the reservoir (**Choi, et al., 2009**). Increasing the carbon dioxide concentration could also increase permeability by acidifying the pH and enhancing mineral dissolution (**Carroll and Knauss, 2005**). In the deeper aquifers, convective mixing and increased salinity can be evidence of increased permeability (**Gunter et al., 1993**). Finally, artificially fracturing the reservoir will open new pathways for fluid transport.

Matter and Kelemen (**2009**) suggest that unconventional storage reservoirs such as fractured basalt and peridotite have the highest potential for carbon dioxide mineralization. Though the rock itself is impermeable, existing intricate fracture patterns allow carbon dioxide to permeate through it. The artificial fracturability of the host rock is quite high as well. The simple silicates are the source for cations with which the injected carbon dioxide reacts to form mineral solids. Basalt and peridotite are geographically significant rocks, so could form large reservoirs. Large reservoirs of permanently sequestered carbonate appear advantageous, but the lack of impermeable seals during the carbonation process may mean that the carbon will escape before fully reacting.

The composition of the injection stream also can play a dominant role in the efficiency of the resultant reservoir. Contaminant gases that remain in from the capturing process (SO_x, NO_x, H_2S) do not have a significant impact on the injection or sequestration, therefore a purified carbon dioxide stream is not requisite for injection. The other gases are common waste products from flue gas, and a large part of the expense of carbon dioxide sequestration, which can be cut

with minor side effect (**Knauss et al., 2005, Palandri and Kharaka, 2005**). In fact, the introduction of sulfur to the carbon dioxide stream can promote the formation of siderite or ankerite mineralization from ferric iron sediments in the unit (**Palandri and Kharaka, 2005**). Patterning carbon dioxide injections with injections of brine can promote the storage of carbon dioxide in enclosed pores, residually trapped by immiscible water along its only escape route. As the carbon dioxide begins to dissolve, pressure and density equilibration will then develop in the reservoir, likely increasing flow capacity (**Qi et al., 2009**).

Current challenges

Geologic disposal of carbon dioxide is technically feasible over several trapping modes, however, there are still challenges to be met. If the sequestered carbon dioxide releases into the atmosphere, becomes a danger or causes damage, the efficacy and worth of the project diminishes.

Injecting carbon dioxide fluid into deep saline aquifers saturated with brine introduces a geomechanical problem. Though the carbon dioxide will slowly dissolve and precipitate, as injection continues, pressure builds in the reservoir. The seal and caprock must be impermeable enough to retain the carbon so it does not migrate out of the reservoir, access a fault or fracture, or release back into the atmosphere (**Ferronato et al., 2010**).

Reservoirs at depth often have a low margin of predictability. Heterogeneity in the reservoir may result in differential pressure on the caprock which could cause buckling or damage the structural integrity of the units above or below. Carbon sequestration reservoirs are often selected very deep (>800 m) to safeguard against this issue (**Zahid et al., 2011**).

Increasing salinity and acidity of brine at depth with more carbon dioxide injection increases the abiity of that fluid to dissolve minerals. This has been cited before as a welcome

increase in permeability and injection efficiency. However, if the acidic fluid dissolves part of the caprock, it could release into shallower aquifers or back into the atmosphere (**Kharaka, 2009**).

If the carbon does leak to the surface, it can harm delicate freshwater ecosystems (**Lu et al., 2009**). The immediate acidification of freshwater through reaction with carbon dioxide will soon be buffered by the dissolution of carbonate and silicate minerals. Though the pH will equilibrate, the over abundance of Ca, Mg, Si, K, Sr, Mn, Ba, Co, B, are permanently elevated, causing the nutrient balance within the freshwater systems to suffer (**Lu et al., 2009; Zahid et al., 2011**).

DISCUSSION

This discussion section integrates the data collected for this study with the reviewed literature. The petrography will be discussed in combination with the lithology and carbon storage chapters.

Diagenetic Heterogeneity

Variability in diagenetic products extends across thin-section, hand sample and outcrop scales. Since diagenesis is so dependent on formation waters and fluid flow, grain texture and mineralogical composition are measureable controls on diagenetic heterogeneity (**Milliken, 2001**). Samples evaluated in this study were carefully selected to be representative of the sandstone bodies whence they came, however, the paragenesis can only reflect observations from the one slice of that sample that ended up on the thin section. How confidently can the paragenetic interpretations be applied to their full lateral extent? This study suggests that since these cross-sections cover a shorter distance than the regional studies and the sandstone bodies are largely uniform in thickness and continuity, the paragenetic relationships can be considered broadly consistent along the lateral extent measured in the cross-sections (**Fig. 5, 6**). Similar patterns in the gamma ray signatures within the sandstone bodies are more distinguishable in some sequences than others, but their traceable presence indicates compositional continuity. Changes in grain texture over the cross-sections were not measured. While there is definitely heterogeneity in mineral composition within and between the sandstone bodies, this evenness suggests a passable predictability in the diagenetic assemblage.

The order of eogenetic alterations are most important for preserving or eliminating primary porosity. The earlier more rigid cements such as silica cement form, the more porosity is preserved and fluid flow pathways propped open. The immature framework grain assemblage in

these continuous sublitharenites and early-onset siderite and chlorite grain coatings deflected major proportions of authigenic silica, which preferentially nucleates on quartz grain surfaces, from forming in the study interval. Without the rigid support, these sandstones were compacted during high rates of sedimentation into the foreland basin, and primary pore space was eliminated.

Morad (**2000**) proposed that eogenetic alterations are somewhat predictable across regions because they are affected by their depositional environments. For example, siderite has been linked to early stages of diagenesis (e.g. **Mozley, 1989; El-ghali et al., 2006**). Reed and others (**2003**) sampled eogenetic siderite and concluded, based on low delO18 in the carbonate, that it formed when still able to mix with surface or ambient waters. Most of the authigenic minerals identified in this study have been attributed to have formed during eodiagenesis, and the interpreted depositional environment is consistent over the study area. Mesogenetic alterations are much more difficult to predict than eogenetic reactions, because they are more dependent on the flow regime in the reservoir than on compositional components coming from the depositional environment (**Morad, 2000**).

Enhanced Coal Bed Methane in Russell County

The Virginia Center for Coal and Energy Research (VCCER) has been involved in ongoing studies to evaluate carbon sequestration in coal bed seams for several years. The capture facility, injection well (BD-114) and monitoring wells (M1 and M2) are built, and have undergone a series of injection tests through the TASK projects. One thousand tons (907 tonnes) of carbon dioxide has been successfully injected over a one-month period, and stimulating the production of methane from the Pocahontas coals (**Ripepi et al., 2011**). It is estimated that in coal seams over the entire central Appalachian basin, 1.3 billion tons of carbon dioxide could be

sequestered in the coal seams. The majority of the storage capacity is in southwestern Virginia, because that is where the net coal is the thickest (**Conrad et al., 2006; Ripepi, 2009**).

The M2 well was used as a monitoring well for the enhanced coal bed methane injection into BD-114. Located approximately 500 ft from the injection well, oriented along the butt cleat of the coal, the M2 was the farthest away of the two monitoring wells, but within the projected carbon dioxide plume distance. Permeability through the coals is very high due to the coal cleat fractures, however, it still took days for the carbon dioxide plume to migrate to the monitoring well (**Ripepi et al., 2011**).

The sandstones associated with the coals have been considered confining units due to their very low permeability. For example, the injected carbon dioxide in the coal beds does not intrude into the sandstone units. Coals mostly abut finer-grained confining units, and it is suggested that diffusive silica cementation from illite-smectite reactions in shale may produce excess silica which migrates into the sandstone and deposits very near the shale-sandstone contact (**McBride, 1989**). Evidence for this cementation pattern was not observed in the study interval, but it is not outside the realm of possibilities if the diagenesis is more heterogeneous than predicted. If shale-derived silica cementation did occur locally, it would certainly decrease the permeability at sandstone contacts with anything finer-grained.

Reservoir Quality

Determining reservoir quality for a carbon sequestration repository is very similar to the quality assessed for a hydrocarbon reservoir. Reservoir quality is merited on the basis of available volume, the strength of the seal, and on the reactivity of the mineral components of the reservoir (**Beard and Meylan, 1987**).

When determining capacity of a reservoir for carbon dioxide, the calculations necessary involve more than just a simple volume calculation (**Bachu and Adams, 2003**). Bradshaw and others (**2007**) list that theoretical, realistic and viable reservoir capacities must be considered for a relevant volume value. *Theoretical capacity* assumes that all open space is accessible to storage, and that all formation water is available to have carbon dioxide dissolved into it at maximum saturation. *Realistic capacity* takes geological and engineering limitations into account when estimating potential capacity. Porosity and permeability, depth of burial, pressure and stress regimes and strength of seal cap. Finally, *viable capacity* considers economic, legal and regulatory barriers of carbon dioxide storage (**Bradshaw et al., 2007**).

Calculating the true *theoretical capacity* of the lower Pennsylvanian sandstones requires more total thickness data than is incorporated in this study. Using the volume estimates from the Regional Lithology chapter (Table 1), multiplied by the measured porosity data from the Petrography chapter, the capacity is 1.15 ± 0.7 km^3 (39.5 ± 24 Bcf) in the region bounded by the two cross-sections from this study.

The *realistic capacity* involves the strength of the seal and the permeability of the unit. Each of the low-frequency sequences contains a thick, named shale. Grimm (**2010**) performed a seal evaluation on the Hensley Shale, just above the Bottom Creek Formation (**Fig. 5**). He determined that the Hensley was an impermeable seal, capable of containing 207 psi before seal failure, and recommended that any carbon dioxide injection take place below that shale, below about 900 ft. Regional correlation of the Hensley Shale shows that it maintains a rather constant thickness in the study area, without major structures compromising the seal (**Grimm, 2010**). Above the Hensley Shale is the Alvy Creek Formation. If the volume potential of Alvy Creek sandstones are removed in the *realistic capacity*, the storage capacity decreases to 0.7 ± 0.4 km^3

(24 ± 14.5 Bcf). These volume estimates do not represent the amount of carbon dioxide that can be stored, only the calculated estimation of available space. Also, the estimates do not account for diagenetic heterogeneity; there may be areas in the sandstone that are markedly more permeable than others.

The permeability of the sandstones is the greatest obstacle to their reservoir quality. Permeabilities less than 10 millidarcies are considered too low to be commercially feasible (**van der Meer and Yavuz, 2009**), but the permeabilities measuredby Grimm (**2010**) from two samples of sublitharenite are 4.6 nanodarcys and 9.2 nanodarcys, respectively. It should be mentioned, though, that the sampled sublitharenites had a porosity of only 3%, which is noticeably less than the average for the sandstones covered in this study.

Flow rates in brine-filled sandstones with permeabilities as low as these would be incredibly slow, decreasing the volume of storage potential by how much carbon dioxide can migrate through the sandstones. Heterogeneous saline aquifers inhibit the trapping of carbon dioxide by blocking the plume migration, but have the capacity to store the carbon dioxide through residual trapping (**Flett et al., 2007**). Regulating the carbon dioxide injection stream would be difficult to manipulate.

At the temperatures and pressures within the Breathitt sandstones, mineral components in the reservoir rocks are not immediately reactive the carbon dioxide due to slow kinetics. Mineralization depends on migration pathways, which determine the framework grains with which carbon dioxide comes in contact (**Bradshaw et al., 2007**). The metals present in the brine will not form mineral solids rapidly enough, due to more acidic waters, for mineralization to become a problem with injection (**Druckenmiller and Maroto-Valer, 2005**).

The sandstones in the study area are shallow relative to deep saline aquifers proposed in other locations. Most literature assumes potential reservoirs will be at or above the supercritical conditions of carbon dioxide (in excess of 7.38 MPa and 31.1 ^{o}C, **Diamond and Akinfiev, 2003**), where carbon dioxide is much more soluble into the brine. In the study area, the pressures and temperatures will be much lower than the expected conditions for carbon sequestration. At ~50^{o}C and >900 ft of depth, fewer reactions occur between the authigenic minerals and carbon dioxide than would at higher temperatures where heat is considered the catalyst. Residual trapping would likely be the dominant form of carbon sequestration (**Flett et al., 2007**). However, any mineral carbonation in these sandstones that does occur could clog up the already scarce pore throats, and drastically reduce the permeability.

Injection of carbon dioxide into saline brine will initially make the solution more acidic, and depending on the equilibrium pH of the system entered, buffer back to a more neutral pH by dissolving framework minerals. Framework grain dissolution may increase permeability, but given the low permeability and pressure and temperature conditions, the reaction time would be prohibitively long rendering injection largely ineffective. However, if the temperature is high (>150^{o}C), the pH of the brine will continue to increase to slightly more basic levels. The more basic the solution, the more likely it is to precipitate mineral carbonates (**Druckenmiller and Maroto-Valer, 2005**).

Drilling an injection well for carbon sequestration is an expensive task. In order for a reservoir to be considered economically viable, is must be able to accept large volumes of carbon dioxide, allow it to migrate to a physical or chemical trap and sequester or store it there. The enhanced coal bed methane project has the added bonus of recovery in the Pocahontas coals which makes them very attractive for financial gain. Injecting carbon dioxide into saline aquifers

is not a “value-added” process, since offset brine is not valuable methane. The sandstones in the lower Pennsylvanian strata in Russell County, while laterally extensive, are not sufficiently permeable to store up economically or environmentally viable quantities of carbon dioxide.

Even with the benefit of ready equipment and an already successful carbon sequestration project, the porosity and permeability are low enough to inhibit the migration of any injected carbon dioxide plume. Realistic capacity is diminished again by the inability for the carbon dioxide to expand within the reservoir, rendering volume calculations irrelevant. Diagenetic alterations to the original framework grain assemblage are ultimately responsible for the poor reservoir quality of the lower Pennsylvanian Breathitt Group sandstones in southwestern Virginia.

Taking this assessment beyond the regional context, foreland basin sandstones close to the thrust front in general experience similar diagenetic conditions (**Galloway, 1984**), and so would have similar reservoir quality issues. Compressible uplifted rock fragments compact around mechanically stable mineral grains deposited in the basin during tectonic- and sediment-loading, dramatically reducing the connectivity of primary porosity. Without sufficient pore space or permeability, rigid cements are not in place early enough to prop open primary pores. However, even mature sandstones in the Appalachian foreland basin have low permeabilities due to an overabundance of silica cements. Tectonic thrusting can bring the basin-fill into contact with warmer fluids from much deeper rocks, which precipitate as they migrate through the cooler basin sediments (**Evans and Battles, 1999; Evans and Hobbs, 2003; Reed et al., 2005**). Given this information, foreland sandstones farther away from the thrust front may have better reservoir quality due to decreased compaction and distance from migrating fluids.

CONCLUSIONS

1- Both high-frequency and low-frequency sequences identified by previous authors in the central Appalachian basin can be extended onto the suite of lower Pennsylvanian strata in Russell County, Virginia. Regional lithology exhibits even stratal patterns across the study area, cross-sections are not broad enough to display basin-scale stacking patterns.

2- Simple predictions of volume indicate that out of the approximately 84 km^3 of rock in the lower Pennsylvanian package below the measured cross-sections, 23 km^3 are laterally extensive basal sands, 14 km^3 are thick, named shales, and the rest are heterolithic facies or coal beds. Seal capacity of the Hensley Shale determined by Grimm (2010) is applied to this volume, since the caprock is mapped consistently along both cross-sections. Estimated realistic capacity of the continuous sandstone bodies below the Hensley Shale is 0.7 ± 0.4 km^3 (24 ± 14.5 Bcf) of brine-filled space.

3- Lower Pennsylvanian sandstones from Russell County, Virginia are sublitharenites comprised mostly (18-45%) of polycrystalline quartz, but with a significant proportion (15-40%) of monocrystalline quartz, and the common occurrence (18-34%) of sedimentary and metamorphic rock fragments. Other framework grains such as feldspars and muscovite comprise 5-8% of the total grain assemblage.

4- Early compaction of framework grains and formation of authigenic minerals such as siderite, chlorite and kaolinite during eodiagenesis lithified the sandstone units. Mesodiagenetic reactions (>70^{o}C) included the onset of localized silica cementation and albitization and illitization of potassium feldspar and metamorphic lithic grains. Late stage calcite cement filled in much of the available pore space.

5- Primary and secondary mineralogies are not reactive with injected carbon dioxide at the temperatures and pressures present in the Breathitt sandstones. Mineralization is unlikely to occur due to increased acidity when carbon dioxide dissolves into formation waters, and the slow kinetics on equilibrium reactions.

6- Secondary moldic and micro-porosity are very low in the sampled sandstones, ranging from 2-9%, with an average of 5%. Permeability measured for these sandstone units by Grimm (**2010**) yields prohibitively low values of 4-9 nanodarcies, which are far below the 10 millidarcy threshold proposed by van der Meer and Yavuz (**2009**).

7- Diagenetic alterations are primarily responsible for the poor reservoir quality of the Breathitt sandstone units. Lower Pennsylvanian sandstones are unlikely candidates for carbon sequestration reservoirs because of their lithologic heterogeneity, low porosity and permeability, and shallow depth.

REFERENCES

Aagaard, P., Egeberg, P., Saigal, G., Morad, S., Byorlykke, K., 1990, Diagenetic Albitization of Detrital K-Keldspars in Jurassic, Lower Cretaceous and Tertiary Clastic Reservoir Rocks from Offshore Norway, II. Formation Water Chemistry and Kinetic Considerations: Journal of Sedimentary Petrology, v. 60, no. 4, p. 575-581.

Allen, J.L., 1993, Lithofacies relations and controls on deposition of fluvial-deltaic rocks of the upper Pocahontas Formation in southern West Virginia: Southeastern Geology, v. 33, p. 131-147.

Alley. R., and others, eds., 2007, Climate Change 2007: The Physical Science Basis: Summary for Policymakers: Intergovernmental Panel on Climate Change, 21 p.

Andrews, J., Brimblecombe, P., Jickells, T., Liss, P. Reid, B., 2004, An Introduction to Environmental Chemistry: Blackwell Publishing, 296 pp., 2nd ed.

Archer, A.W., and Greb, S.F., 1995, An Amazon-scale Drainage System in the Early Pennsylvanian of Central North America, The Journal of Geology, v. 103, p. 611-628.

Arkle, T. Jr., 1974, Stratigraphy of the Pennsylvanian and Permian Systems of the Central Appalachians *in* Stratigraphy of the Central Appalachians: GSA Special Paper 148.

Baccar, M. B., Fritz, B., and Madé, B., 1993, Diagenetic albitization of K-feldspar and plagioclase in sandstone reservoirs: thermodynamic and kinetic modeling: Journal of Sedimentary Petrology, v. 63, no. 6, p. 1100-1109.

Bachu, S., Gunter, W., and Perkins, E., 1994, Aquifer Disposal of CO2: Hydrodynamic and Mineral Trapping: Energy Conversion Management, v. 35, no. 4, p. 269-279.

Bachu, S., Adams, J., 2003, Sequestration of CO2 in geological media in response to climate change: capacity of deep saline aquifers to sequester CO2 in solution: Energy Conversion and Management, v. 44, pp. 3151-3175.

Beard, R., and Meylan, M., 1987, Petrology and hydrocarbon reservoir potential of subsurface Pottsville (Pennsylvanian) sandstones, Black Warrior Basin, Mississippi.

Biddle, K., and Wielchowsky, C., 1994, Hydrocarbon Traps, *in* Magoon, L., and W. G. Dow, eds., The Petroleum System- from source to trap: AAPG Memoir 60, p. 219-235.

Bjørkum, P., Walderhaug, O., and Aase, N., 1993, A model for the effect of illitization on porosity and quartz cementation of sandstones: Journal of Sedimentary Petrology, v. 63, no. 6, pp1089-1091.

Bjørkum, P., 1996, How important is pressure in causing dissolution of quartz in sandstones: Journal of Sedimentary Geology, v. 66, no. 1, pp. 147-154.

Blackmer, G.C., Omar, G.I., and Gold, D. P., 1994, Post-Alleghanian unroofing history of the Appalachian Basin, Pennsylvania, from apatite fission track analysis and thermal models, Tectonics, v. 13, no. 5, pp1259-1276.

Blake, B. M., and Beuthin, J.D., 2008, Deciphering the mid-Carboniferous eustatic event in the central Appalachian foreland basin, southern West Virginia, USA *in* Fielding, C.R., Frank, T.D., and Isbell, J.L., eds., Resolving the Late Paleozoic Ice Age in Time and Space: Geological Society of America Special Paper 441, pp249-260.

Blakey, R. C., 2008, Gondwana paleogeography from assembly to breakup—A 500 m.y. odyssey *in* Fielding, C.R., Frank, T.D., and Isbell, J.L., eds., Resolving the Late Paleozoic Ice Age in Time and Space: Geological Society of America Special Paper 441, pp1-28.

Blair, T., and Bilodeau, W., 1988, Development of tectonic cyclothems in rift, pull-apart, and foreland basins: Sedimentary response to episodic Tectonism: Geology, v. 16, pp. 517-520.

Bodek, R. J., 2006, Sequence stratigraphic architecture of early Pennsylvanian, coal-bearing strat of the Cumberland block: a case study from Dickenson county, Virginia: [M.S. thesis] Virginia Polytechnic Institute and State University, 84pp.

Boettcher, S.S., and Milliken, K.L., 1994, Mesozoic-Cenozoic unroofing of the southern Appalachian basin: apatite fission track evidence from Middle Pennsylvanian sandstones: Journal of Geology, v. 102, p. 655-663.

Bradshaw, J., Bachu, S., Bonijoly, D., and others, 2007, CO2 storage capacity estimation: Issues and development of standards: International Journal of Greenhouse Gas Control, v. 1, p. 62-68.

Bruhn, F., Bruckschen, P., Richter, D., Meijer, J., Stephan, A., and Veizer, J., 1995, Diagenetic history of sedimentary carbonates: Constraints from combined cathodoluminescence and trace element analyses by micro-PIXE: Nuclear Instruments and Methods in Physics Research B, v. 104, p. 409-414.

Budd, D., Hammes, U., and Ward, W., 2000, Cathodoluminescence in calcite cements: new insights on Pb and Zn sensitizing, Mn activation, and Fe quenching at low trace-element concentrations: Journal of Sedimentary Research, v. 70, no.1, p. 217-226.

Bustin, R., and Clarkson, C., 1998, Geological Controls on coalbed methane reservoir capacity and cas content: International Journal of Coal Geology, v. 38, p. 3-26.

Byørlykke, K., and Egeberg, P.K., 1993, Quartz cementation ion Sedimentary Basins: AAPG Bulletin, v. 77, no. 9, pp. 1538-1548.

Carroll, S., and Knauss, K., 2005, Dependence of labradorite dissolution kinetics on CO2(aq), Al(aq), and temperature: Chemical Geology, v. 217, pp. 213-225.

Castle, J.W., 2001, Appalachian basin stratigraphic response to convergent-margin structural evolution: Basin Research, v. 13, p. 397-418.

Cecil, C.B., 1990, Paleoclimate controls on stratigraphic repetition of chemical and siliciclastic rocks, Geology (Boulder), v. 18, p. 533-536.

Chen, C., and Goodell, H.G., 1964, The petrology of Lower Pennsylvanian Sewanee sandstone, Lookout Mountain, Alabama and Georgia: Journal of Sedimentary Geology, v. 34, no.1, pp.46-72.

Chesnut, D. R., 1994, Eustatic and tectonic control of deposition of the lower and middle Pennsylvanian strata of the central Appalachian Basin, *in* Dennison, J.M. and Ettensohn, F.R., eds. Tectonic and eustatic controls on sedimentary cycles: SEPM Special Publication no. 4, pp51-64.

Chesnut, D. R., 1996, Geologic framework for the coal-bearing rocks of the Central Appalachian Basin, International Journal of Coal Geology, v.31, pp55-66.

Choi, H., Yun, S., Koh, Y., Mayer, B., Park, S. and Hutcheon, I., 2009, Geochemical behavior of rare-earth elements during the evolution of CO2-rich groundwater: A study from the Kangwon district, South Korea: Chemical Geology, v. 262, p. 318-327.

Churnet, H.G., 1996, Depositional environments of Lower Pennsylvanian coal-bearing siliciclastics of southeastern Tennessee, northwestern Georgia, and northeastern Alabama, USA: International Journal of Coal Geology, v. 31, p. 21-54.

Conrad, J.M., Miller, M.J., Phillips, J., Ripepi, N., 2006, Characterization of Central Appalachian Basin CBM Development: Potential for Carbon Sequestration and Enhanced CBM Recovery, *2006 International Coal bed Methane Symposium*, Preprint 0625, Tuscaloosa, AL.

Curtis, C. D., 1978, Possivle links between sandstone diagenesis and depth-related geochemical reactions occurring in enclosing mudstones: Journal of the Geological Society of London, v. 135, pp. 107-117.

Deer, W., Howie, R., and Zussman, J., 2001, Rock Forming Minerals: Framework Silicates: Feldspars: Geological Society Publishing House, 973 pp., 2nd ed.

Davis, M. W., and Ehrlich, R., 1974, Late Paleozoic Crustal Composition and Dynamics in the Southeastern United States, The Geological Society of America, Inc., Special Paper 148, pp171-185.

Davydov, Y., Wardlaw, B., and Gradstein, F., 2004, The Carboniferous Period, *in* A Geologic Time Scale 2004, eds. Felix M. Gradstein, James G. Ogg, and Alan G. Smith, Cambridge University Press, p. 222-248.

De Ros, L.F., Morad, S., and Paim, P.S.G., 1994, The role of detrital composition and climate on the diagenetic evolution of continental molasses: evidence from the Cambro-Ordovician Guaritas Sequence, southern Brazil: Sedimentary Geology, v. 92, p. 197-228.

de Souza, R.S., De Ros, L.F., and Morad, S., 1995, Dolomite diagenesis and porosity preservation in lithic reservoirs: Carmópolis Member, Sergipe-Alagoas Basin, northeastern Brazil: American Association of Petroleum Geologists, Bulletin, v. 79, no. 5, p. 725-748.

Denning, S. F., 2008, Architectural models for lower Pennsylvanian strata in Dickenson/Wise county, southwestern Virginia: a reservoir case study: [M.S. thesis] Virginia Polytechnic Institute and State University, 108pp.

Diamond, L., Akinfiev, N., 2003, Solubility of CO2 in water from -1.5 to 100 oC and from 0.1 to 100 MPa: evaluation of literature data and thermodynamic modeling: Fluid Phase Equilibria, v. 208, pp. 265-290.

Dickinson, W.R., and Suczek, C.A., 1979, Plate Tectonics and Sandstone Compositions: AAPG Bulletin, v. 63, no. 12, pp. 2164-2182.

Dickinson, W. R., Beard, L. S., Brakenridge, G. R., Erjavec, J. L., Ferguson, R. C., Inman, K. F., Knepp, R. A., Lindberg, F. A., and Ryberg, P. T., 1983, Provenance of North American Phanerozoic sandstones in relation to tectonic setting: Geol. Soc. America Bull., v. 94, p. 222-235.

Dickinson, W. R., 1985, Interpreting provenance relations from detrital modes of sandstones, *in* Zuffa, G. G., ed., Provenance of arenites: Dordrecht, Netherlands, D. Reidel Publishing Company, p. 333–361.

Donaldson, A.C., Renton, J. J., and Presley, M.W., 1985,Pennsylvanian deposystems and paleoclimates of the Appalachians, International Journal of Coal Geology, v. 5, pp167-193

Druckenmiller, M., and Maroto-Valer, M., 2005, Carbon sequestration using brine of adjusted pH to form mineral carbonates: Fuel Processing Technology, v. 86, p. 1599-1614.

Eble, C.F., 1996, Lower and lower Middle Pennsylvanian coal palynofloras, southwestern Virginia: International Journal of Coal Geology, v. 31, p. 67-113.

Ehrenberg, S.N., Aagaard, P., Wilson, M.J., Faser, A.R., and Duthie, D.M.L., 1993, Depthdependent transformation of kaolinite to dickite in sandstones of the Norwegian continental shelf: Clay Minerals, v. 28, p. 325-352.

El-ghali, M.A.K., et al., 2006, Origin and timing of siderite cementation in Upper Ordovician glaciogenic sandstones from the Murzuq basin, SW Libya: Marine and Petroleum Geology, v. 23, pp. 459-471.

Englund, K.J., Arndt, H.H., and Henry, T.W., 1979, Proposed Pennsylvanian system stratotype, Virginia and West Virginia: [Falls Church, Va., American Geological Institute], v. 136 pp.

Englund, K.J., Windolph, J.F., Jr., and Thomas, R.E., 1986, Origin of thick, low-sulphur coal in the Lower Pennsylvanian Pocahontas Formation, Virginia and West Virginia: Special Paper Geological Society of America, v. 210, p. 49-61.

Englund, K.J., and Thomas, R.E., 1990, Late Paleozoic depositional trends in the central Appalachian Basin: U. S. Geological Survey Bulletin, Report: B.

Ennis-King, J., and Paterson, L., 2007, Coupling of geochemical reactions and convective mixing in the long-term geological storage of carbon dioxide: International Journal of Greenhouse Gas Control, p. 86-93.

Eriksson, K.A., Campbell, I.H., Palin, J.M., Allen, C.M., and Bock, B., 2004, Evidence for Multiple Recycling in Neoproterozoic through Pennsylvanian Sedimentary Rocks of the Central Appalachian Basin, Journal of Geology, v.112, pp261-276.

Evans, M.A., and Battles, D.A., 1999, Fluid inclusion and stable isotope analyses of veins from central Appalachian Valley and Ridge province: implications for regional synorogenic hydrologic structure and fluid migration: Geological Society of America Bulletin, v. 111, no. 12, p. 1841-1860.

Evans, M.A., and Hobbs, G.C., 2003, Fate of 'warm' migrating fluids in the central Appalachians during the Late Paleozoic Alleghanian orogeny: Journal of Geochemical Exploration, v. 78-79, p. 327-331.

Ferm, J.C., and Horne, J.C., 1979, Carboniferous depositional environments in the Appalachian region: [Columbia, Dept. of Geology, University of South Carolina], vi, 760 pp.

Ferronato, M., Gambolati, G., Janna, C., and Teatini, P., 2010, Geomechanical issues of anthropogenic CO2 sequestration in exploited gas fields: Energy Conversion and Management, v. 51, p. 1918-1928.

Flett, M., Gurton, R., and Weir, G., 2007, Heterogeneous saline formations for carbon dioxide disposal: Impact of varying heterogeneity on containment and trapping: Journal of Petroleum Scienc and Engineering, v. 57, p. 106-118.

Folk, R., 1974, The natural history of crystalline Calcium Carbonate: Effect of magnesium content and salinity

Galehouse, J.S., 1971, Point counting, *in* Carver, R.E., ed., Procedures in Sedimentary Petrology: New York, pp385-408.

Galloway, W.E., 1974, Deposition and Diagenetic Alteration of Sandstone in Northeast Pacific Arc-related basins: Implications for Graywacke Genesis: GSA Bulletin, v. 85, p. 379-390.

Galloway, W.E., 1984, Hydrogeologic regimes of sandstone diagenesis, in D.A. McDonald and R.C. Surdam, eds., Clastic Diagenesis: American Association Petroleum Geologists Memoir 37, p. 3-13.

Gilfillan, S., Lollar, B., Holland, G., and others, 2009, Solubility trapping in formation waters as dominant CO2 sink in natural gas fields: Nature, v. 458, p. 614-618.

Goldstein, R.H., and Reynolds, T.J., 1994, Systematics of fluid inclusions in diagenetic minerals, Society of Economic Paleontologists and Mineralogists, Short Course 31, 199 p.

Götze, J., 2009, Chemistry, textures and physical properties of quartz – geological interpretation and technical application: Mineralogical Magazine, v.73, no. 4, p. 645-671.

Greb, S.F., and Chesnut, D.R., 1996, Lower and lower Middle Pannsylvanian fluvial to estuarine deposition, central Appalachian basin: Effects on eustasy, tectonics, and climate, GSA Bulletin, v.108, no. 3, pp303-317.

Greb, S.F., and Martino, R.L., 2005, Fluvial-estuarine transitions in fluvial-dominated successions; examples from the Lower Pennsylvanian of the Central Appalachian Basin: Special Publication of the International Association of Sedimentologists, v. 35, p. 425-451.

Greb, S.F., et al., 2008, Appalachian sedimentary cycles during the Pennsylvanian: Changing influences of sea level, climate and tectonics *in* Fielding, C.R., Frank, T.D., and Isbell, J.L., eds., Resolving the Late Paleozoic Ice Age in Time and Space: Geological Society of America Special Paper 441, pp235-248.

Grimm, R.P., 2010, Insights into the stratigraphic evolution of the early Pennsylvanian Pocahontas Basin, Virginia [Ph.D. thesis]: Virginia Polytechnic Institute and State University, 243 pp.

Gunter, W., Perkins, E., and McCann, T., 1993, Aquifer Disposal of CO2-rich Gases: Reaction Design for Added Capacity: Energy Conversion Management, v. 34, no. 9-11, p. 941-948.

Gunter, W., Perkins, E., and Hutcheon, I., 2000, Aquifer disposal of acid gases: modeling of water-rock reactions for trapping of acid wastes: Applied Geochemistry, v. 15, p. 1085-1095.

Hatcher, R.D., Jr., 2002, Alleghanian (Appalachian) orogeny, a product of zipper tectonics: Rotational, transpressive continent–continent collision and closing of ancient oceans along irregular margins, *in* Martínez Catalán, J.R., Hatcher, R.D., Jr., Arenas, R., and Díaz García, F., eds., Variscan-Appalachian dynamics: The building of the Late Paleozoic basement: Boulder, Colorado, Geological Society of America Special Paper 364, p. 199–208.

Hellevang, H., et al., 2005, Can Dawsonite Permanently Trap CO2?: Environmental Science Technology, v. 39, pp. 8281-8287.

Hiatt, E., and Kyser, K., 2000, Links between depositional and diagenetic processes in basin analysis: porosity and permeability in sedimentary rocks, *in* Kyser, K., ed., Fluids and Basin Evolution: Mineralogical Association of Canada, Short Course Series 28, p. 63-92.

Houseknecht, D.W., 1978, Pottsville Quartzarenites and Greywackes [Ph.D. thesis]: Pennsylvania State University, 197 p.

Houseknect, D.W., 1980, Comparative anatomy of a Pottsville lithic arenite and quartz arenite of the Pocahontas Basin, southern West Virginia: petrogenetic, depositional, and stratigraphic implications, Journal of Sedimentary Geology, v.50, no.1, pp3-20

Houseknecht, D.W., 1984, Influence of grain size and temperature on intergranular pressure solution, quartz cementation, and porosity in a quartzose sandstone: Journal of Sedimentary Petrology, v. 54, no. 2, pp. 348-361.

Houseknecht, D.W., 1988, Intergranular pressure solution in four quartzose sandstones: Journal of Sedimentary Petrology, v. 58, no. 2, pp. 228-246.

Hulver, M.L., 1997, Post-orogenic Evolution of the Appalachian Mountain System and its Foreland [Ph.D. Thesis]: Chicago, University of Chicago, 1055 p.

Issler, D., Grist, A., Stasiuk, L., 2005, Post-Early Devonian thermal constraints on hydrocarbon source rock maturation in the Keele Tectonic Zone, Tulita area, NWT, Canada, from multi-kinetic apatite fission track thermochronology, vitrinite reflectance and shale compaction: Bulletin of Canadian Petroleum Geology, v. 53, no. 4, p. 405-431.

Jeans, C.V., 2000, Mineral diagenesis and reservoir quality – the way forward: an introduction: Clay Minerals, v. 35, p. 3-4.

Kang-Min, Y., Boggs, S., Seyedolali, A., and Jaehong, K., 1997, Albitization of feldspars in sandstones from the Gohan (Permian) and Donggo (Permo-Triassic) formations, Gohan area, Kangwondo, Korea: Geoscience Journal (Seoul), v. 1, no. 1, p. 26-31.

Kastner, M., 1971, Authigenic feldspars in carbonate rocks: American Mineralogist, v. 56, p. 1403-1442.

Kastner, M., and Siever, R., 1979, Low temperature feldspars in sedimentary rocks: American Journal of Science, v. 279, p. 435-479.

Kaszuba, J., Janecky, D., and Snow, M., 2005, Experimental evaluation of mixed fluid reactions between supercritical carbon dioxide and NaCl brine: Relevance to the integrity of a geologic carbon repository: Chemical Geology, v. 217, pp. 277-293.

Kharaka, Y., Thorrdsen, J., Hovorka, S., Nance, H., Cole, D., Phelps., T., and Knauss, K., 2009, Potential environmental issues of CO2 storage in deep saline aquifers: Geochemical results from the Frio-I Brine Pilot test, Texas, USA: Applied Geochemistry, v. 24, p. 1106-1112.

Klein, G.deV., and Willard, D.A., 1989, Origin of the Pennsylvanian bearing cyclothems of North America: Geology v. 17, no. 2, p. 152-155.

Knauss, K., Johnson, J., Steefel, C., 2005, Evaluation of the impact of CO2, co-contaminant gas, aqueous fluid and reservoir rock interactions on the geologic sequestration of CO2: Chemical Geology, v. 217, pp. 339-350.

Korus, J.T., 2002, The lower Pennsylvanian New River Formation: a non-marine record of glacioeustasy in a foreland basin, Masters thesis, Virginia Polytechnic Institute and State University

Korus, J.T., 2002, The lower Pennsylvanian New River Formation a nonmarine record of glacioeustasy in a foreland basin: [M.S. thesis] Virginia Polytechnic Institute and State University, 61pp.

Korus, J.T., Kvale, E.P., Eriksson, K.A., and Joeckel, R.M., 2008, Compound paleovalley fills in the Lower Pennsylvanian New River Formation, West Virginia, USA: Sedimentary Geology, v. 208, p. 15-26.

Kurlenya, M., and Serdyukov, S., 2010, Methane desorption and migration in thermodynamic inequilibrium coal beds: Journal of Mining Science, v. 46, no. 1, p. 61-68.

Langmuir, D., 1997, Aqueous Environmental Geochemistry: Prentice Hall, Upper Saddle River, New Jersey, 600 p.

Lanson, B., Beaufort, D., Berger, G., Bauer, A., Cassagnabère, A., and Meunier, A., 2002, Authigenic kaolin and illitic minerals during burial diagenesis of sandstones: a review: Clay Minerals, v. 37, p. 1-22.

Levine, J.R., and Davis, A., 1989, The relationship of coal optical fabrics to Alleghanian tectonic deformation in the central Appalachian fold-and-thrust belt, Pennsylvania: Geological Society of America Bulletin, v. 101, no. 10, p. 1333-1347.

Lu, J., Partin, J., HoVorka, S., Wong, C., 2010, Potential risks to freshwater resources as a result of leakage from CO2 geological storage: a batch-reaction experiment: Environmental Earth Science, v. 60, p. 335-348.

Lyons, P. C.; Krogh, T. E.; Kwok, Y. Y.; and Zodrow, E. L. 1997. U-Pb age of zircon crystals from the upper Banner tonstein (middle Pennsylvanian), Virginia: absolute age of the Lower Pennsylvanian-Middle Pennsylvanian boundary and depositional rates for the Middle Pennsylvanian, central Appalachian basin. *In* Podemski, M.; Dybova, J. S.; Jaworowski, K.; Jureczka, J.; and Wagner, R., eds. Proceedings of the XIII International Congress on the Carboniferous and Permian (Prace Panstwowego Instytut Geologicznego, 157). Warsaw, Prace Panstwowy Instytut Geologiczny, p. 159–166.

Lyons, P.C. 1998. The central and northern Appalachian Basin—a frontier region for coal bed methane development. International Journal of Coal Geology, v. 38 p. 61–87

Lyons, P.C., T.E. Krogh, Y.Y. Kwok, D.W. Davis, W.F. Outerbridge, H.T. Evans Jr., 2006, Radiometric ages of the Fire Clay tonstein [Pennsylvanian (Upper Carboniferous), Westphalian, Duckmantian]: A comparison of U-Pb zircon single-crystal ages and 40Ar/39Ar

Macaulay, C. I., Haszeldine, R.S., and Fallick, A.E., 1993, Distribution, chemistry, isotopic composition and origin of diagenetic carbonates: Magnus sandstone, North Sea: Journal of Sedimentary Petrology, v. 63, no. 1, pp. 33-43.

Matter, J., and Kelemen, P., 2009, Permanent storage of carbon dioxide in geological reservoirs by mineral carbonation: Nature Geoscience, v. 2, p. 837-841.

McBride, E., 1989, Quartz Cement in Sandstones: A Review: Earth-Science Reviews, v. 26, p. 69-112.

McDowell, R.J., 1986, An interpretation of the Grafton sandstone and its implications for Pennsylvanian paleohydraulics, climate, provenance, and tectonics: Compass of Sigma Gamma Epsilon, v. 63, no. 2, p. 48-57.

Michael, K., Golab, A., Shulakova, V., Ennis-King, G., Sharma, S., Aiken, T., 2010, Geological Storage of CO2 in saline aquifers- A review of the experience from existing storage operations: International Journal of Greenhouse Gas Control, v.4, p. 659-667.

Milici, R.C., Ryder, R.T., Swezey, C.S., Charpentier, R.R., Cook, T.A., Crovelli, R.A., Klett, T.R., Pollastro, R.M., and Schenk, C.J., 2003, Assessment of Undiscovered Oil and Gas Resources of the Appalachian Basin Province, 2002: U.S. Geological Survey Fact Sheet FS-009-03, 4 p.

Miller, J.D., and Kent, D.V., 1988, Regional trends in the timing of Alleghanian remagnetization in the Appalachians: Geology, v. 16, no. 7, p. 588-591.

Milliken, K., 2001, Diagenetic heterogeneity in sandstone at the outcrop scale, Breathitt Formation (Pennsylvanian), eastern Kentucky: AAPG Bulletin, v. 85, no. 5, pp. 795-815.

Milliken, K., 2003, Microscale distribution of a kaolinite in Breathitt Formation sandstones (middle Pennsylvanian): implications for mass balance: International Association of Sedimentology Special Publication 34, pp. 343-360.

Morad, S., Ketzer, J., and De Ros, L., 2000, Spatial and temporal distribution of diagenetic alterations in siliciclastic rocks: implications for mass transfer in sedimentary basins: Sedimentology, v. 47 (Suppl. 1), pp.95-120.

Mozley, P.S., 1989, Relation between depositional environment and the elemental composition of early diagenetic siderite: Geology, v. 17, pp. 704-706.

Mukhopadhyay, P., 1994, Vitrinite Reflectance as Maturity Parameter: Petrographic and Molecular Characterization and its Applications to Basin Modeling: Americal Chemical Society Symposium series, p. 1-24.

Nolde, J.E., Spears, D. 1998. A preliminary assessment of in place coal bed methane resources in the Virginia portion of the central Appalachian Basin, International Journal of Coal Geology, v. 38 p.115–136.

Palandri, J. Kharaka, Y., 2005, Ferric iron-bearing sediments as a mineral trap for CO2 sequestration: Iron reduction using sulfur-bearing waste gas: Chemical Geology, v. 217, pp. 351-364.

Pashin., J.C., Groshong Jr., R.H., Carroll, R.E., 2001, Enhanced Coal bed Methane Recovery Through Sequestration of. Carbon Dioxide: Potential for a Market-Based Environmental. Solution in the Black Warrior Basin of Alabama.

Pashin, J. C., 2004, Cyclothems of the Black Warrior Basin, Alabama, U.S.A.: Eustatic snapshots of foreland basin tectonism, in J. C. Pashin and R. A. Gastaldo, eds., Sequence stratigraphy, paleoclimate, and tectonics of coal-bearing strata: AAPG Studies in Geology 51, p. 199 –218.

Pettijohn, F., Potter, P., and Siever, R., 1972, Sand and Sandstone: Springer-Verlag Press, 618 pp.

Portier, S., and Rochelle, C., 2005, Modelling CO2 solubility in pure water and NaCl-type waters from 0 to 300 oC and from 1 to 300 bar: Application to the Utsira Formation at Sleipner: Chemical Geology, v. 217, no. 3-4, p. 187-199.

Primmer, T.J., Cade, C.A., Evans, J., Gluyas, J.G., Hopkins, M.S., Oxtoby, N.H., Smalley, P.C., Warren, E.A., and Worden, R.H., 1997, Global patterns in sandstone diagenesis: their application to

reservoir quality prediction for petroleum exploration, in Kupecz, J.A., Gluyas, J., and Bloch, S., eds., Reservoir quality prediction in sandstones and carbonates: American Association of Petroleum Geologists, Memoir 69, p. 61-77.

Pryer, L., and Robin, P., 1996, Differential stress control on the growth and orientations of flame perthite: a paleostress-direction indicator: Journal of Structural Geology, v. 18, no. 9, p. 1151-1166.

Qi, R., LaForce, T., Blunt, M., 2009, Design of carbon dioxide storage in aquifers: International Journal of Greenhouse Gas Control, v.3, p.195-205.

Quinlan, G.M., and Beaumont, C., 1984, Appalachian thrusting, lithospheric flexure, and the Paleozoic stratigraphy of the Eastern Interior of North America, Canadian Journal of Earth Sciences, v.21, pp973-996.

Ramseyer, K., Boles, J., and Lichtner, P., 1992, Mechanism of Plagioclase Albitization: Journal of Sedimentary Petrology, v. 62, no. 3, p. 349-356.

Reed, J.S., Eriksson, K. A., and Kowalewski, M., 2005a, Climatic, depositional and burial controls on diagenesis of Appalachian Carboniferous sandstones: qualitative and quantitative methods: Sedimentary Geology, v. 176, pp225-246.

Reed, J.S., Spotila, J.A., Eriksson, K.A., and Bodnar, R.J., 2005b, Burial and Exhumation history of Pennsylvanian strata, central Appalachian basin: an integrated study, Basin Research, v. 17, pp259-268.

Richter, D., Götte, Th., Götze, J., and Neuser, R., 2003, Progress in application of cathodoluminescence (CL) in sedimentary petrology: Mineralogy and Petrology, v. 79, p. 127-166.

Ripepi, Nino Samuel, 2009, Carbon dioxide storage in coal seams with enhanced coalbed methane recovery geologic evaluation, capacity assessment and field validation of the Central Appalachian Basin: [Ph. D. thesis] Virginia Polytechnic Institute and State University, 237 pp.

Ripepi, N., Karmis, M., and B. Kelley, 2011, Characterization and Field Validation of the Carbon Sequestration Potential of Coal Seams in the Central Appalachian Basin: Virginia Center for Coal and Energy Research, Final Report submitted to the U.S. Department of Energy, National Energy Technology Laboratory in partial fulfillment of contract DE-FC26-05NT42590.

Rice, C.L., 1985, Terrestrial vs. marine depositional model—A new assessment of subsurface Lower Pennsylvanian rocks of southwestern Virginia: Geology, v.13, pp786-789.

Rice, C.L., and Schwietering, J.F., 1988, Fluvial deposition in the Central Appalachians during the Early Pennsylvanian: U. S. Geological Survey Bulletin, Report: B.

Rouse, W. R., 2006, Sequence stratigraphy and architecture of Lower Pennsylvanian strata, southern West Virginia: potential for carbon sequestration and enhanced coal-bed methane recovery in the Pocahontas Basin: [M.S. thesis] Virginia Polytechnic Institute and State University, 84pp.

Ruppert, L., Hower, J., Ryder, R., and others, 2010, Geologic controls on thermal maturity patterns in Pennsylvanian coal-bearing rocks in the Appalachian basin: International Journal of Coal Geology, v.81, p. 169-181.

Saigal, G.C., Morad, S., Bjørlykke, K., Egeberg, P. K., and Aagaard, P., 1988, Diagenetic albitization of detrital K-feldspar in Jurassic, Lower Cretaceous, and Tertiary clastic reservoir rocks from offshore Norway, I. Textures and origin: Journal of Sedimentary Petrology, v. 58, no. 6, p. 1003-1013.

Scotese, C. R., 2004, A Continental Drift Flipbook:Journal of Geology, v. 112, p.729-741.

Shi, J., Mazumder, S., Wolf, K. and Durucan, S., 2008, Competitive Methane Desorption by Supercritical CO2 Injection in Coal: Transportation of Porous Media, v. 75, p. 35-54.

Sibley, D. F., and Blatt, H., 1976, Intergranular pressure solution and cementation of the Tuscarora Orthoquartzite: Journal of Sedimentary Petrology, v. 46, no. 4, pp. 881-896.

Siever, R., 1957, Pennsylvanian sandstones of the Eastern-Interior coal basin; Jour. Sed.

Petrology, v. 27, p. 227-250.

Spötl, C., Houseknecht, D., and Longstaffe, F., 1994, Authigenic chlorites in sandstones as indicators of high-temperature diagenesis, Arkoma Foreland Basin, USA: Journal of Sedimentary Research, v. A64, no. 3, p. 553-566.

Tankard, A.J., 1986, Depositional Response to Foreland Deformation in the Carboniferous of Eastern Kentucky, AAPG Bulletin, v. 70, no. 7, pp853-868.

Tans, P. and Keeling, R., 2011, Trends in atmospheric carbon dioxide: Recent monthly CO2 at Mauna Loa, Hawaii, http://www.esrl.noaa.gov/gmd/ccgg/trends/, retrieved 06/27/2011.

Tenthorey, et al., 1998, Precipitation sealing and diagenesis, Experimental results: Journal of Geophysical Research, v. 103, no. B10, p. 915-23.

Van der Meer, L., Yavuz, F., 2009, CO2 storage capacity calculations for the Dutch subsurface: Energy Procedia, v.1, p.2615-2622.

Van der Voo, R., 1983, A plate tectonics model for the Paleozoic assembly of Pangea based on paleomagnetic data, *in* Hatcher, R.D. Jr., Williams, H., and Zietz, I., eds., Contributions to the tectonics and geophysics of mountain chains: Geological Society of America Memoir 158, p. 19-24.

Vernon, R., 1999, Flame perthite in metapelite gneisses at Cooma, SE Australia: American Mineralogist, v. 84, p. 1760-1765.

Voll, G., 1960, New work on petrofabrics: Liverpool and Manchester Geological Journal, v. 2, n. 3, p.503-567.

von Eynatten, H., Barcelo-Vidal, C., Pawlowsky-Glahn, V., 2003, Composition and Discrimination of Sandstones: A Statistical Evaluation of Different Analytical Methods: Journal of Sedimentary Research, v.73, pp. 47-57.

Walker, T., 1984, Diagenetic Albitization of Potassium Feldspar in Arkosic Sandstones: Journal of Sedimentary Petrology, v. 54, no. 1, p. 3-16.

White, C., Smith, D., Jones, K., and others, 2005, Sequestration of Carbon Dioxide in Coal with Enhanced Coalbed Methane Recovery – A Review: Energy & Fuels, v. 19, no. 3, p. 659-724.

Wilson, M.D., ed., 1994, Reservoir Quality Assessment and Prediction in Clastic Reservoirs: SEPM Short Course 30, 432 p.

Wizevich, M. C., 1991, Sedimentology and regional implications of fluvial quartzose sandstones of the Lee Formation, central Appalachian basin: [Ph.D. thesis] Virginia Polytechnic Institute and State University, Blacksburg.

Xu, T., Apps, J., and Pruess, K., 2005, Mineral sequestration of carbon dioxide in a sandstone-shale system: Chemical Geology, v. 217, pp. 295-318.

Young, S., 1976, Petrographic Textures of Detrital Polycrystalline Quartz as an aid to interpreting Crystalline Source Rocks: Journal of Sedimentary Petrology, v. 46, no. 3, p. 595-603.

Zahid, U., Lim, Y., Jung, J., Han, C., 2011, CO2 geological storage: A review on present and future prospects: Korean Journal of Chemical Engineering, v. 28, no. 3, p. 674-685.

APPENDIX A: Petrographic Data

Sample	Qm	Qp	Fk	Fp	Lm	Ls	Musc	Biot	Seri	Chl	Org	Zirc/Tour	Ps	Sil	Sid	Calc	Kaol	Ill	Chlc
M2-421	14	81	0	14	50	0	9	1	3	1	3	0	8	0	3	10	1	0	2
M2-426	63	34	7	10	40	0	1	0	4	1	4	0	13	0	16	2	6	1	3
M2-441	77	35	3	11	40	0	4	0	2	4	3	0	7	1	7	0	6	0	0
M2-512	76	35	13	15	30	0	0	0	0	2	0	1	21	0	1	5	2	0	0
M2-524.5	30	68	3	12	61	3	1	2	6	1	0	0	10	0	2	0	1	0	0
M2-533	81	39	2	12	26	0	2	0	1	2	1	0	22	0	5	7	0	0	0
M2-555	86	38	12	7	29	0	1	0	0	1		0	8	1	4	14	0	0	0
M2- 581.2	27	73	11	13	34	7	2	0	1	2	1	0	21	0	7	1	0	0	0
M2-620	20	108	3	14	36	0	3	0	6	2	1	0	4	0	2	1	1	0	0
M2-645	65	45	4	12	23	10	2	0	0	0	4	0	24	1	4	4	3	0	0
M2-745	22	74	0	12	59	5	7	4	3	3	1	1	9	0	0	0	0	0	0
M2-775	74	52	10	11	26	9	0	0	0	0	1	0	23	2	1	0	0	0	0
M2-786	34	77	10	14	33	1	2	1	1	1	0	0	17	0	5	4	0	0	0
M2-795	30	65	19	23	35	2	0	0	0	2	0	0	23	0	1	0	0	0	0
M2-944	74	40	8	18	25	10	4	1	2	1	0	0	14	2	0	0	1	1	0
M2-971	56	35	11	12	28	0	4	1	1	1	2	0	1	0	0	48	0	0	0
M2-999.9	41	91	12	12	29	1	0	1	3	0	0	0	6	0	2	2	0	0	0
M2-1000	18	110	8	12	34	2	0	0	2	0	0	0	12	0	1	2	0	0	0
M2-1211	76	32	1	4	64	6	1	0	3	1	4	0	0	1	4	1	2	1	0
M2-1217	47	70	0	0	58	2	2	0	8	0	5	2	1	0	2	2	1	0	0
M2-1217.1	41	52	0	1	52	1	8	0	5	0	3	0	9	0	28	0	1	1	0
M2-1228	32	66	0	4	64	5	7	0	7	1	5	0	3	0	0	1	5	0	0
M2-1394	90	32	0	3	42	4	4	0	3	0	6	0	4	0	1	0	0	12	0
M2-1421	24	104	0	12	44	2	0	0	1	0	2	0	11	0	0	0	0	0	0
M2-1439	19	100	0	21	35	4	0	0	3	0	0	0	10	0	1	7	0	0	0

Qm-monocrystalline quartz; Qp-polycrystalline quartz; Fk-Kfeldspar (detrital); Fp-plagioclase feldspar (detrital); Lm-metamorphic rock fragments; Ls-sedimentary rock fragments; Musc-muscovite; Biot-biotite; Seri-sericite; Chl- chlorite (detrital); Org-organic; Zirc/Tour-zircon and tourmaline (detrital); Ps-secondary porosity; Sil-authigenic quartz cement; Sid-siderite; Calc-calcite; Kaol-kaolinite; Ill-illite cement; Chlc-authigenic chlorite.

Sample	Qm	Qp	Fk	Fp	Lm	Ls	Musc	Biot	Seri	Chl	Org	Zirc/Tour	Ps	Sil	Sid	Calc	Kaol	Ill	Chlc
M2-1491	20	108	1	15	26	4	0	0	2	1	2	0	18	0	3	0	0	0	0
M2-1538	20	94	0	12	47	2	0	0	5	0	0	0	2	0	2	13	3	0	0
M2-1627	59	20	0	3	43	15	9	0	3	0	2	1	2	0	40	1	0	2	0
M2-1642	21	96	0	4	42	1	3	1	0	1	0	0	18	0	9	4	0	0	0
M2-1646	58	44	2	14	39	14	4	0	5	0	0	0	19	0	1	0	0	0	0
M2-1646.2	69	54	0	6	32	9	1	1	1	0	1	1	19	0	4	2	0	0	0
M2-1707.5	40	25	0	8	39	4	10	2	6	2	1	0	2	0	59	0	2	0	0
M2-1787	67	27	0	8	57	11	3	2	5	8	6	1	6	0	5	0	0	0	0
M2-1809	21	111	0	12	35	2	1	0	0	0	1	0	7	0	0	10	0	0	0
M2-1821	43	66	0	10	50	3	2	0	1	0	1	0	23	0	1	0	0	0	0
M2-1840	59	38	0	12	32	1	4	1	2	4	8	0	2	0	6	32	0	0	0
M2-1846	49	84	1	5	31	8	4	0	3	2	0	0	1	0	7	4	1	0	0
M2-1890	69	44	2	14	41	5	3	2	5	4	3	1	3	0	3	1	0	0	0
M2-1897	51	62	0	9	37	6	2	1	3	1	2	0	19	0	1	3	3	0	0
M2-1900	46	73	0	12	35	13	1	2	4	2	0	0	4	0	0	2	7	0	0
M2-1931	61	32	0	7	73	4	2	1	5	2	4	0	11	1	0	0	0	0	0
M2-1931.2	42	78	0	11	40	5	2	0	8	3	1	0	11	0	0	0	0	0	0
M2-1955	43	59	0	11	46	11	6	2	3	3	1	0	12	0	1	0	0	0	2
M2-1980	49	59	0	9	39	8	3	1	5	1	0	0	12	0	14	0	0	0	0
M2-2001	43	65	0	9	48	5	4	1	4	1	0	0	10	0	6	3	0	0	1
M2-2013	18	55	0	10	38	70	2	0	0	0	1	0	4	0	1	1	0	1	0
M2-2046.5	93	34	0	2	52	4	1	0	1	0	1	0	10	0	2	1	0	0	0
M2- 2060	84	54	1	3	34	13	3	0	0	0	0	0	7	0	1	0	1	0	0
M2- 2072	54	51	6	1	43	12	2	0	1	2	1	0	12	0	15	0	0	0	0
M2-2123	49	49	0	7	56	14	4	0	7	2	2	1	3	0	6	0	0	0	0
M2-2140	51	46	0	14	56	4	4	1	7	2	3	0	6	0	6	0	0	0	0

Qm-monocrystalline quartz; Qp-polycrystalline quartz; Fk-Kfeldspar (detrital); Fp-plagioclase feldspar (detrital); Lm-metamorphic rock fragments; Ls-sedimentary rock fragments; Musc-muscovite; Biot-biotite; Seri-sericite; Chl- chlorite (detrital); Org-organic; Zirc/Tour-zircon and tourmaline (detrital); Ps-secondary porosity; Sil-authigenic quartz cement; Sid-siderite; Calc-calcite; Kaol-kaolinite; Ill-illite cement; Chlc-authigenic chlorite.